원자분자겨울학교
대전, 카이스트, 2022. 2. 9 - 11

GIST



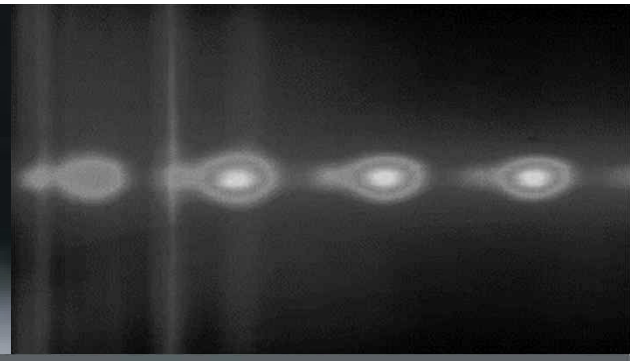

원자분자 겨울학교

극초단 레이저 원자 물리 I

김경택

부교수, 물리광과학과, 광주과학기술원
부연구단장, 초강력레이저과학 연구단, 기초과학연구원

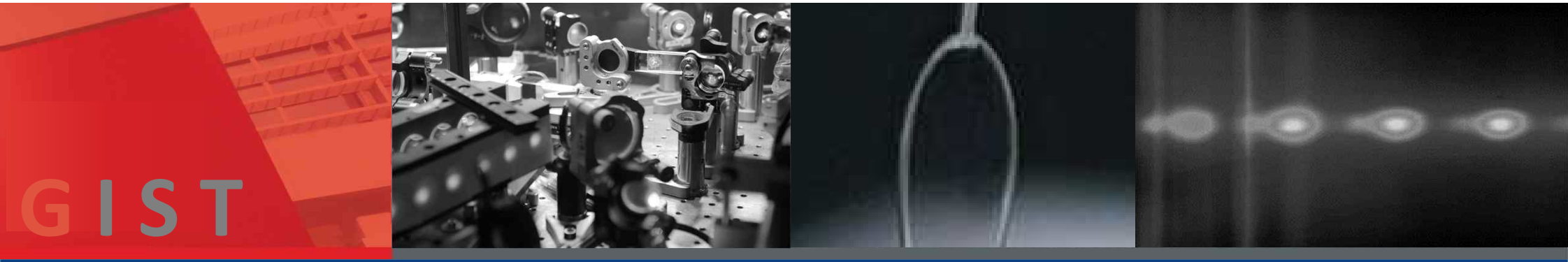

Above threshold ionization

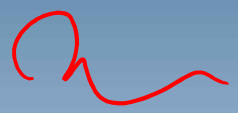

Light-matter interaction

- 'Strong' field physics
  - After tunneling, the field strength of a laser pulse is stronger (or comparable) to the Coulomb field.
  - Therefore the Coulomb field can be neglected.

$I = 10^{13}\ 10^{14}\ (10^{15}\ [W/cm^2]$

- Electron in a strong laser field
  - Ionization
  - Acceleration
  - Rescattering or recombine

- Above threshold ionization
- High harmonic generation
  - Attosecond pulse generation, characterization, and applications
- Frustrated tunneling ionization

Multiphoton vs tunneling ionization

- Keldysh parameter $\gamma = \sqrt{\varepsilon_P / 2U_p}$

* Ponderomotive energy (cycle averaged K.E.)

$$U_P = \frac{e^2}{2m}\langle \mathbf{A}(t)^2 \rangle_T,$$

$$U_p\ [\mathrm{eV}] = 0.09337 I[\mathrm{W/cm^2}]\,\lambda^2[\mathrm{m}]$$

① Multiphoton ionization

② Tunneling ionization

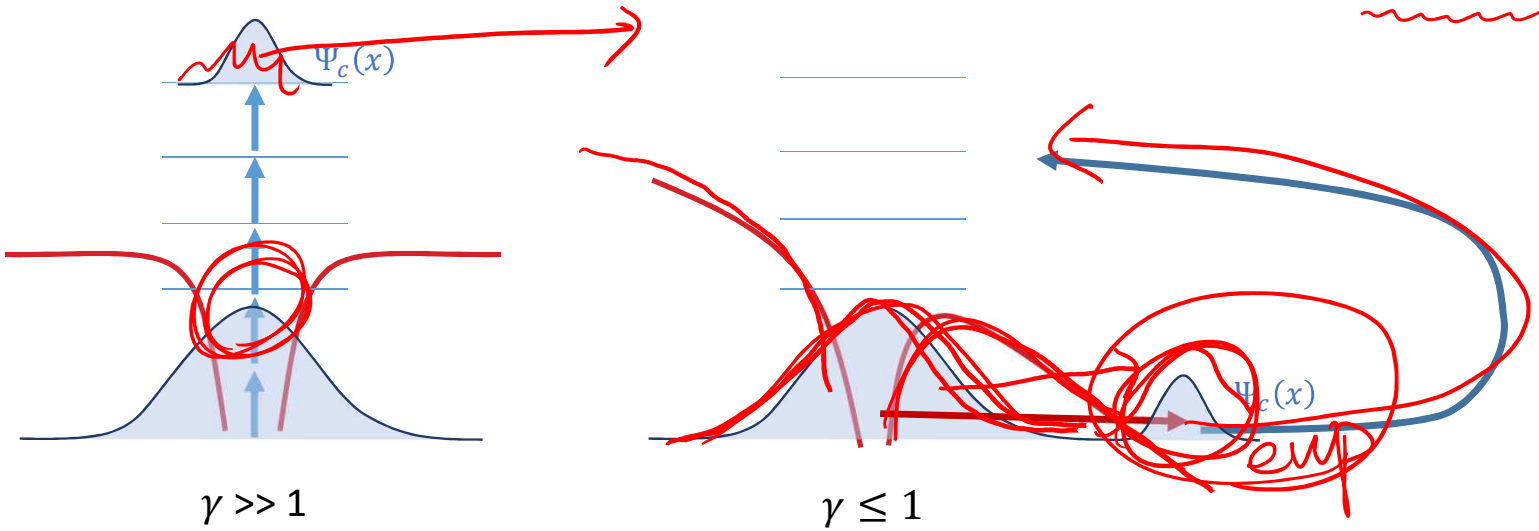

$\gamma >> 1$

$\lambda \downarrow$

$I \downarrow$

$\gamma \leq 1$

$\lambda \uparrow$

$I \uparrow$

$I = 10^{14}$

$0.09 \times 10^{14} \times 10^{-12}$

$= 10$

$\gamma = \sqrt{15\mathrm{eV}/20\mathrm{eV}}$

$\sim 1.$

Tunneling ionization from atoms in a strong laser field

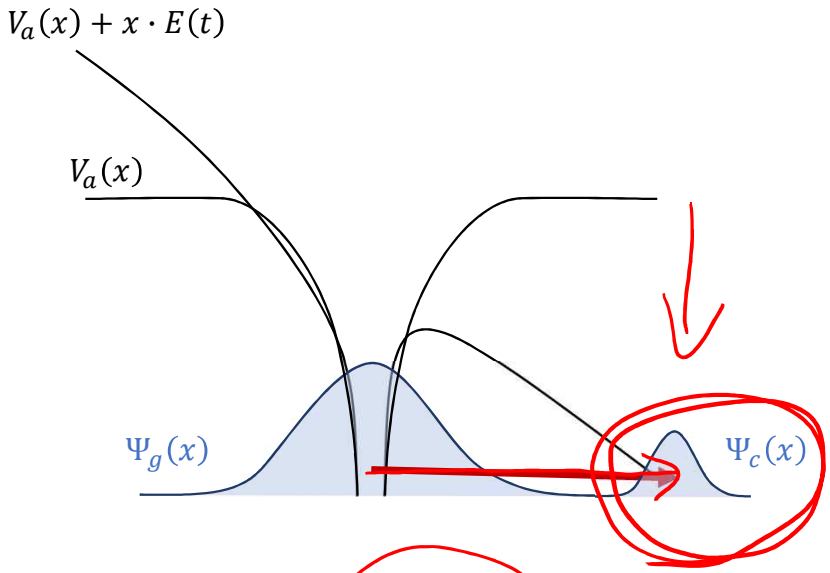

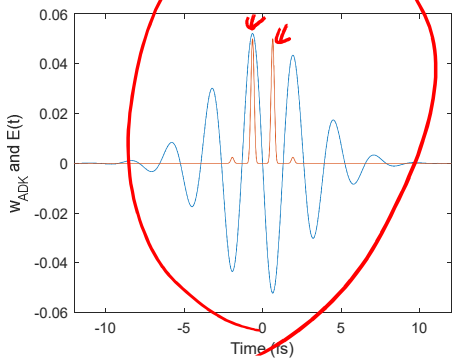

Landau's tunnel ionization rate

$$w = 4\omega_a \frac{E_a}{|E|} \exp\left[-\frac{2}{3}\frac{E_a}{|E|}\right]$$

Hydrogen & DC field

Ammosov-Delone-Krainov (ADK) tunneling rate (Perelomov et al., 1966, Ammosov et al., 1986)

$$\Gamma(t) = AE_{\mathrm{IP}} \left(\frac{4\sqrt{2E_{\mathrm{IP}}^3}}{|\mathcal{E}(t)|}\right)^{2n^* - |m| - 1} \exp\left(-\frac{4\sqrt{2E_{\mathrm{IP}}^3}}{3|\mathcal{E}(t)|}\right)$$

- The ADK model uses the instantaneous electric field E(t).
- N* is the effective principal quantum number.
- The constant A depends on the actual and the effective quantum numbers.
- Assumption: low laser frequency, no excited state, tunneling regime $\gamma = \sqrt{E_{IP}/2U_p}$.

Classical descript of electron trjectories

- Electron trajectories

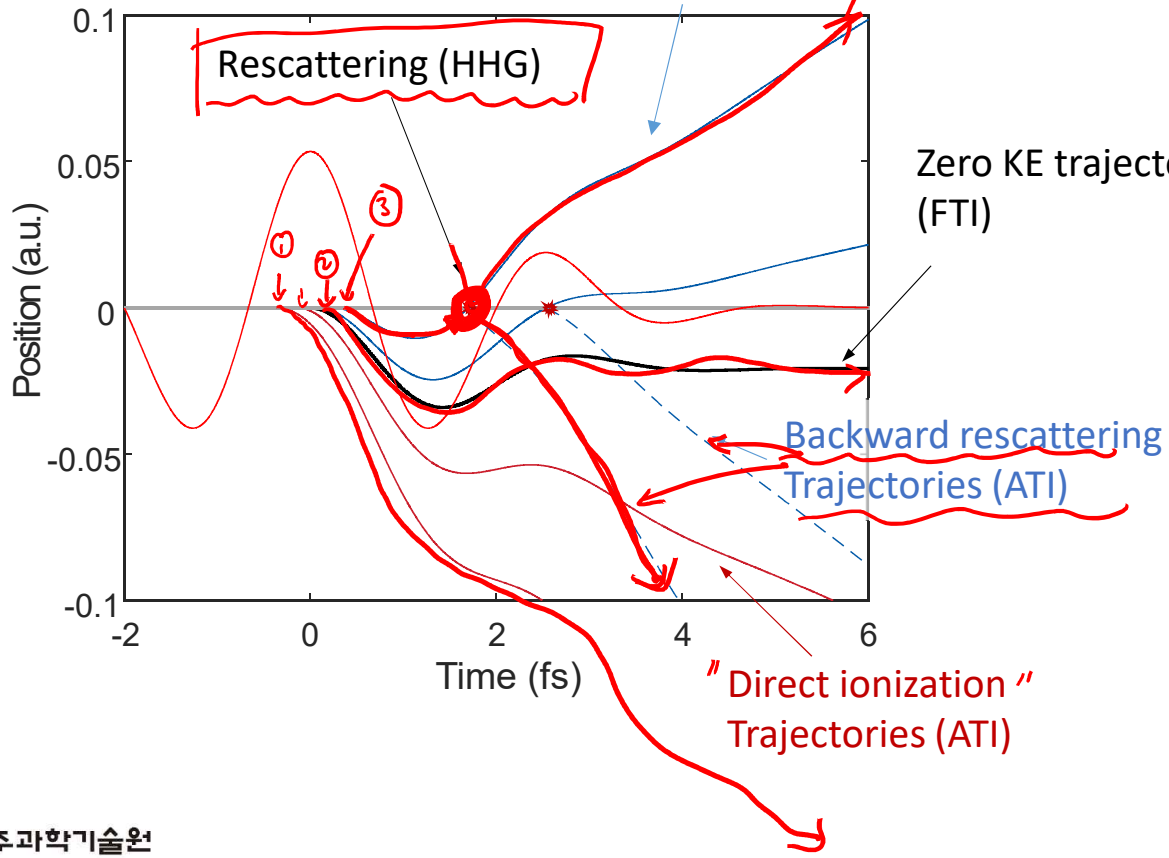

$$v(t) = -\int_{t=t_i}^{+\infty} E(t)\,dt$$

$$x(t) = \int_{t=t_i}^{+\infty} v(t)\,dt$$

Discovery of above threshold ionization

Free-Free Transitions Following Six-Photon Ionization of Xenon Atoms

P. Agostini, F. Fabre, G. Mainfray, and G. Petite
Centre d'Etudes Nucléaires de Saclay, Service de Physique Atomique, 91190 Gif-sur-Yvette, France

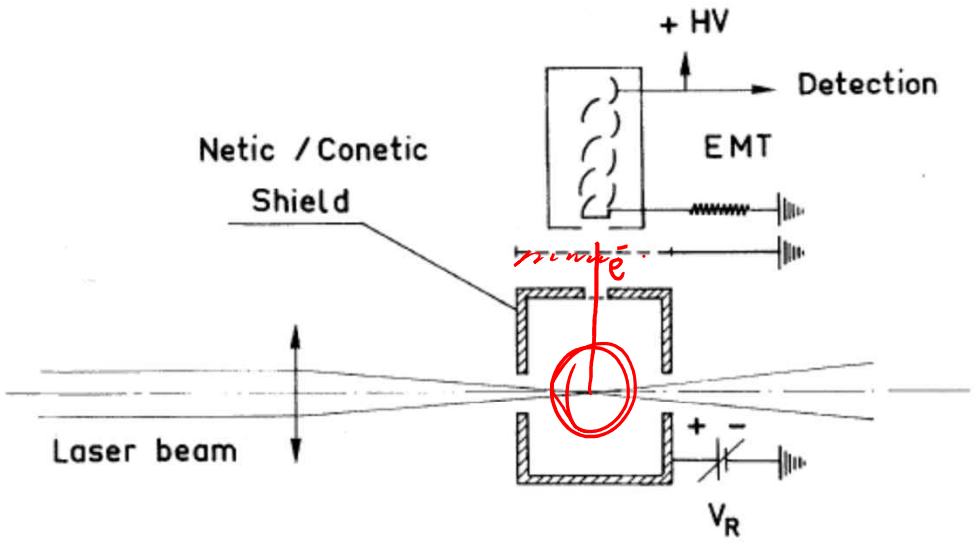

FIG. 2. Schematic of the experimental apparatus.

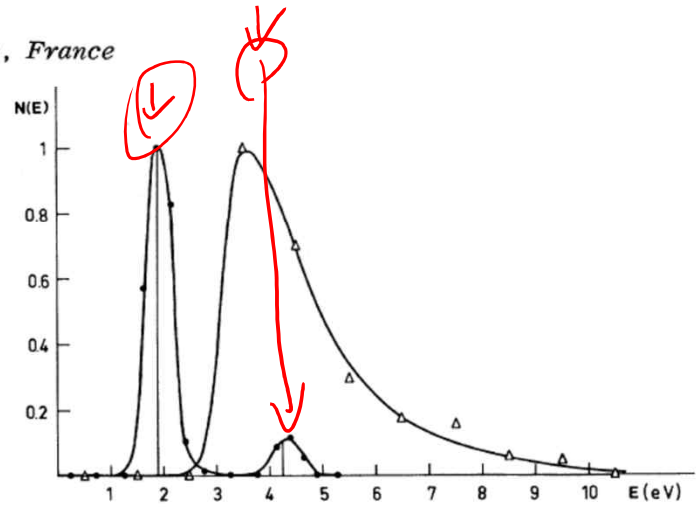

FIG. 3. Energy spectra of the emitted electrons for two photon energies: triangles, $\hbar\omega = 1.17$ eV, $I = 4\times10^{13}$ W/cm^{-2}, $E_{max} = 4$ eV; circles, $\hbar\omega = 2.34$ eV, $I = 8\times10^{12}$ W/cm^{-2}, $E_{max} = 0.2$ eV (E_{max} is the maximum energy gained in the field gradient). The solid straight lines at 1.90 and 4.25 eV have heights proportional to the values of $(d\sigma^{(m)}/d\Omega)\,(d\sigma^{(el)}/d\Omega)^{-1}$ calculated from Eq. (3) using an intensity of 1.0×10^{13} W/cm^{-2}. The solid curves have been hand drawn through the experimental points.

P. Agostini et al., Free-free transitions ..., PRL **42**, 1127 (1979).

Strong field approximation (with saddle point approximation)

- Probability amplitude

$$M_{\mathbf{p}} = \lim_{t \to \infty,\ t' \to -\infty} \langle \psi_{\mathbf{p}}(t) | U(t,t') | \psi_0(t') \rangle$$

$$H(t) = -\frac{1}{2m}\nabla^2 - e\mathbf{r}\cdot\mathcal{E}(t) + V(\mathbf{r})$$

- Approximations
  - Volkov state instead of the scattering states

$$|\psi_{\mathbf{p}}^{(\mathrm{Vv})}(t)\rangle = |\mathbf{p} - e\mathbf{A}(t)\rangle e^{-iS_{\mathbf{p}}(t)}$$

$$\langle \mathbf{r} | \mathbf{p} - e\mathbf{A}(t)\rangle = (2\pi)^{-3/2} \exp i[(\mathbf{p} - e\mathbf{A}(t))\cdot\mathbf{r}$$

$$S_{\mathbf{p}}(t) = \frac{1}{2m}\int^t d\tau\, [\mathbf{p} - e\mathbf{A}(\tau)]^2$$

- Strong field approximation

$$M_{\mathbf{p}} = -i\int_{-\infty}^{\infty} dt_0 \langle \psi_{\mathbf{p}}^{(\mathrm{Vv})}(t_0) | H_I(t_0) | \psi_0(t_0)\rangle$$

Electron born at t0

The electron no longer feels V(r)

- Saddle point approximation

$$\frac{d}{dt}[E_{\mathrm{IP}}t + S_{\mathbf{p}}(t)] = E_{\mathrm{IP}} + \tfrac{1}{2}[\mathbf{p} - e\mathbf{A}(t)]^2 = 0.$$

- Solution

$$M_{\mathbf{p}} \propto \sum_n \delta\left(\frac{\mathbf{p}^2}{2m} + E_{\mathrm{IP}} + U_P - n\omega\right) \times \sum_s \left(\frac{2\pi i}{S_{\mathbf{p}}''(t_s)}\right)^{1/2} e^{i[E_{\mathrm{IP}}t_s + S_{\mathbf{p}}(t_s)]} \langle \mathbf{p} - e\mathbf{A}(t_s) | V | \psi_0 \rangle$$

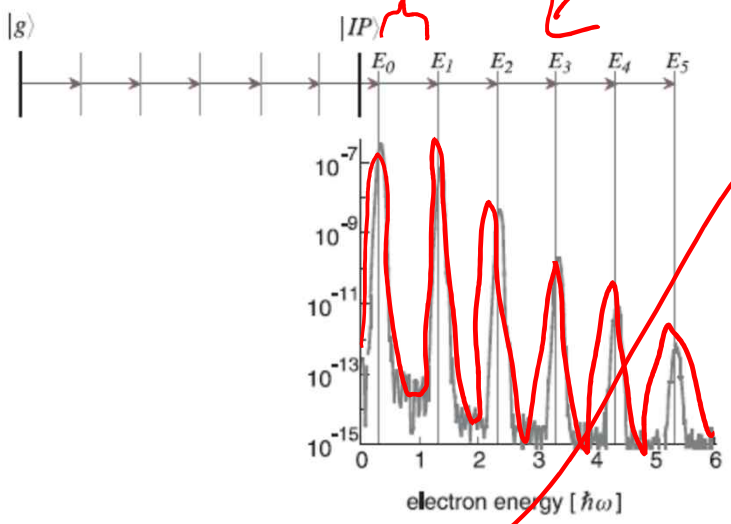

Fig. 1. Photoelectron spectrum in the above-threshold-ionization (ATI) intensity regime. The series of peaks corresponds to the absorption of photons in excess of the minimum required for ionization. The figure shows the result of a numerical solution of the Schrödinger equation (Paulus, 1996).

- Solution

$$M_{\mathbf{p}} \propto \sum_n \delta\left(\frac{\mathbf{p}^2}{2m} + E_{\mathrm{IP}} + U_P - n\omega\right)$$

$$\times \sum_s \left(\frac{2\pi i}{S''_{\mathbf{p}}(t_s)}\right)^{1/2} e^{i[E_{\mathrm{IP}} t_s + S_{\mathbf{p}}(t_s)]} \langle \mathbf{p} - e\mathbf{A}(t_s) | V | \psi_0 \rangle$$

Time-dependent Schrodinger equation

- TDSE with SAE (Single active electron) approximation

$$\frac{-\hbar^2}{2m}\frac{\partial^2\Psi(x,t)}{\partial x^2}+U(x)\Psi(x,t)=i\hbar\frac{\partial\Psi(x,t)}{\partial t}$$

- TDSE (1d)

$$V=\frac{1}{\sqrt{x^2+a_2}}$$

$$\Psi(t+\Delta t)=e^{-\boldsymbol{H}\,(t)}\Psi(t)$$

  - Crank-Nicholson method can be used for stable propagation

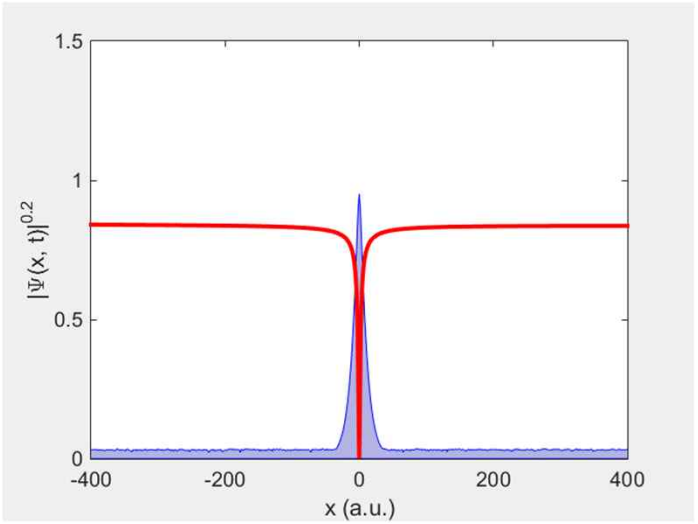

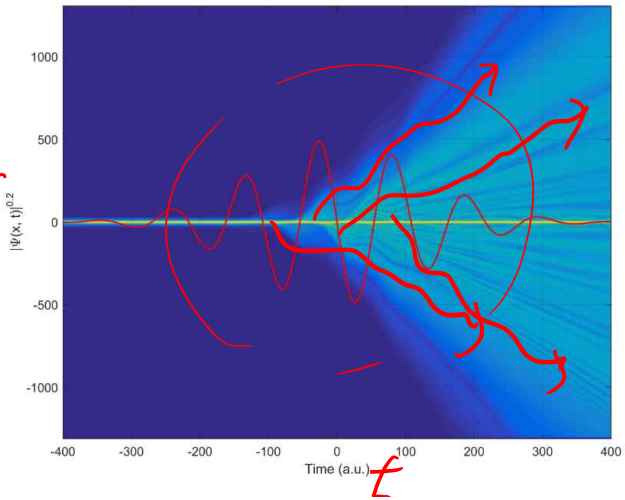

Direct and indirect ionization

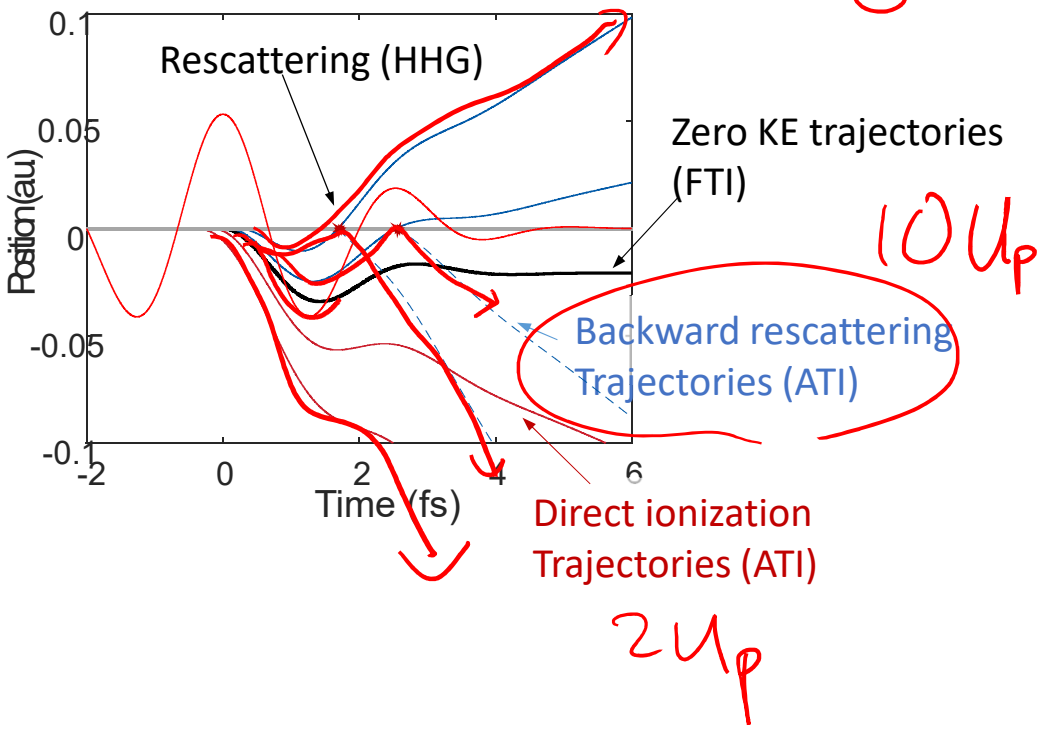

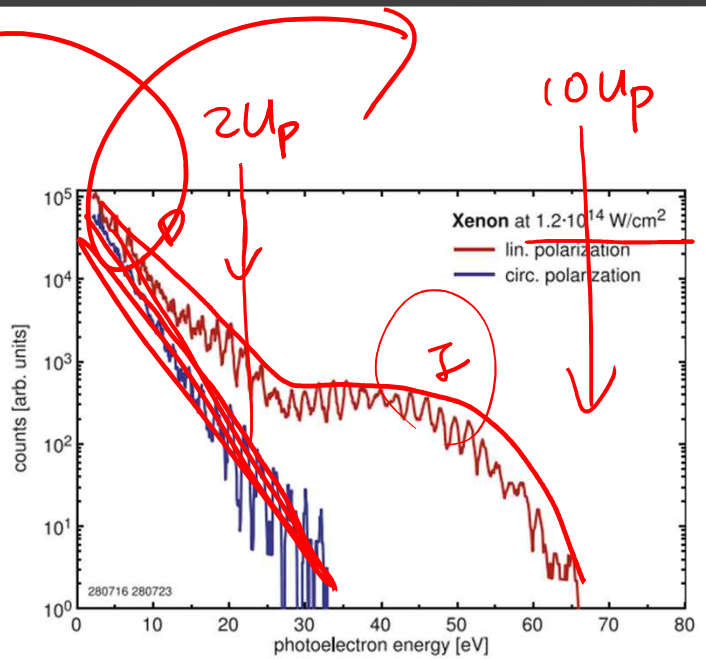

Figure 1. ATI spectra recorded in July 1993 using a femtosecond laser system consisting of a dye colliding-pulse mode-locked oscillator and a dye amplifier pumped by a copper-vapor laser. The wavelength was 630 nm, the pulse duration 40 fs, and the intensity corresponded to $U_p = 4.5$ eV. Besides the ATI plateau and its disappearance for circular polarization, also some of the effects referred to in the main text are visible, in particular varying ATI peak contrast and peak separations not equal to the photon energy.

Absolute phase detection using ATI electrons

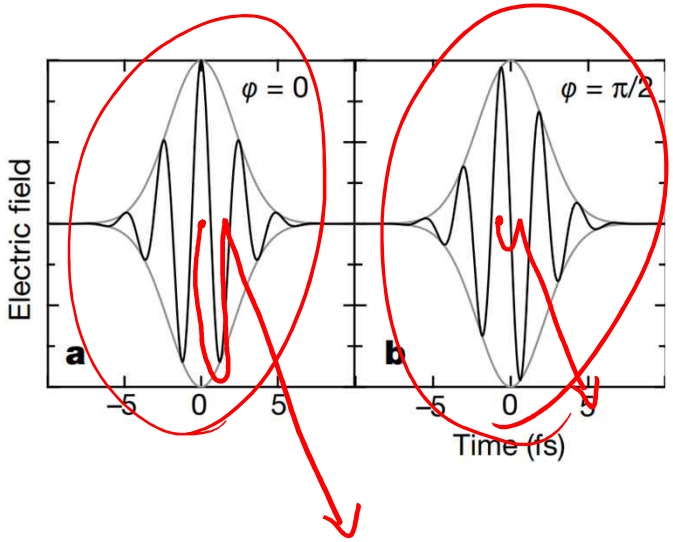

G. G. Paulus et al., Nature **414**, 182 (2001).

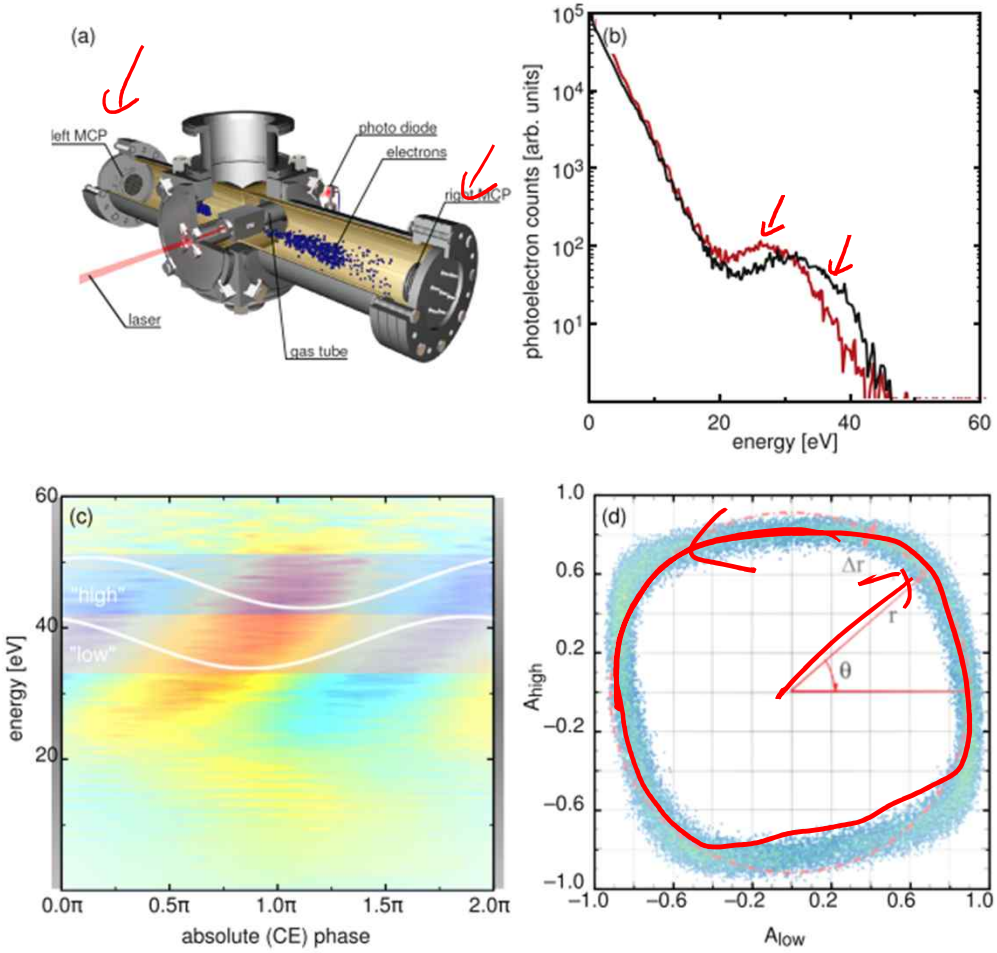

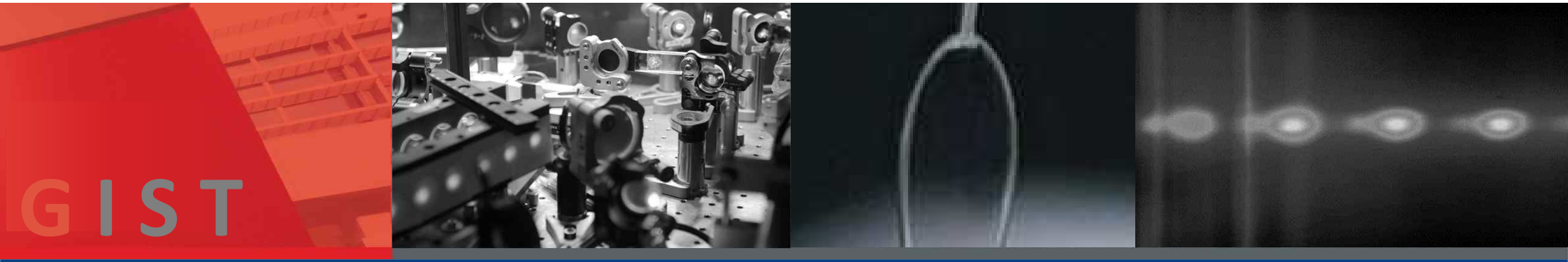

High harmonic generation

Direct and indirect ionization

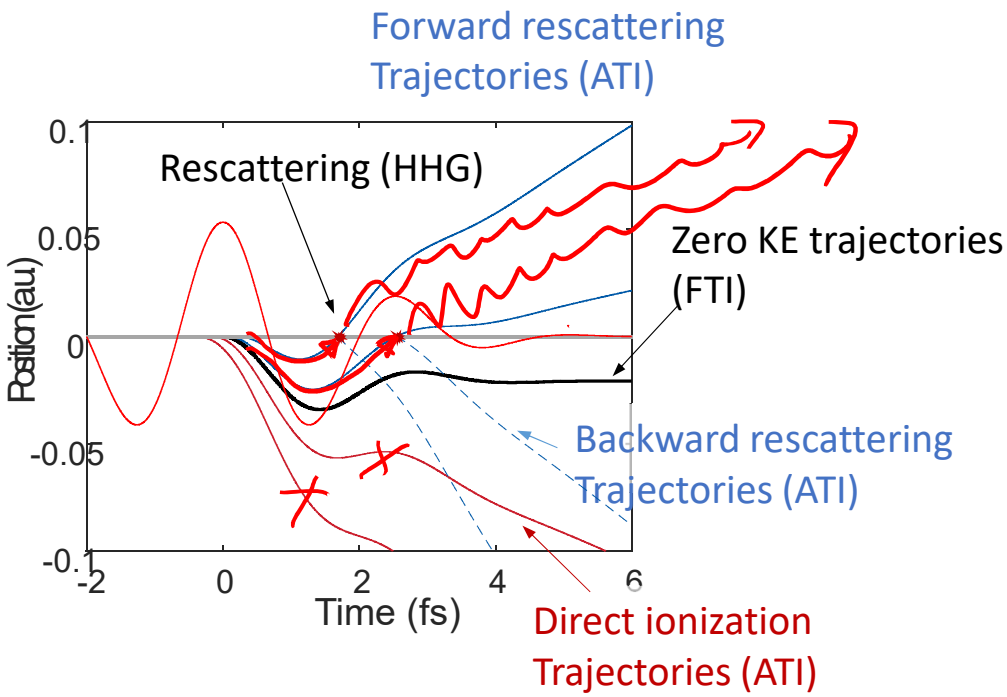

High harmonic generation (semi-classical 3-step model)

- Ionization, acceleration, and recombination

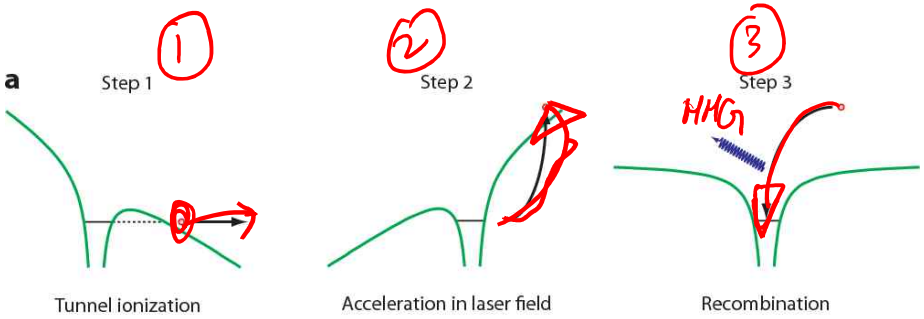

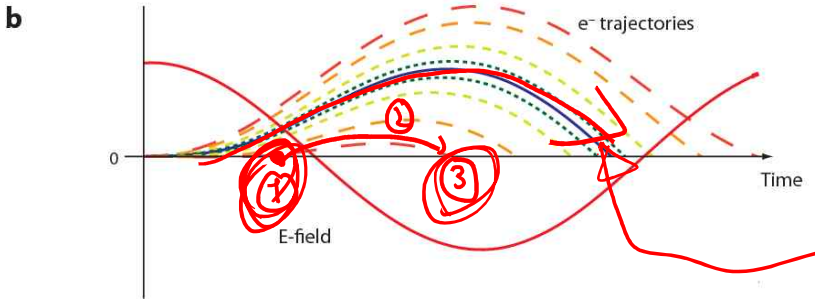

VOLUME 71, NUMBER 13 PHYSICAL REVIEW LETTERS 27 SEPTEMBER 1993

Plasma Perspective on Strong-Field Multiphoton Ionization

P. B. Corkum
National Research Council of Canada, Ottawa, Ontario, Canada K1A 0R6
(Received 9 February 1993)

During strong-field multiphoton ionization, a wave packet is formed each time the laser field passes its maximum value. Within the first laser period after ionization there is a significant probability that the electron will return to the vicinity of the ion with very high kinetic energy. High-harmonic generation, multiphoton two-electron ejection, and very high energy above-threshold-ionization electrons are all consequences of this electron-ion interaction. One important parameter which determines the strength of these effects is the rate at which the wave packet spreads in the direction perpendicular to the laser electric field; another is the laser polarization. These will be crucial parameters in future experiments.

PACS numbers: 32.80.Rm

$$x = x_0[-\cos(\omega t)] + v_{0x}t + x_{0x},$$

$$v_x = v_0 \sin(\omega t) + v_{0x}$$

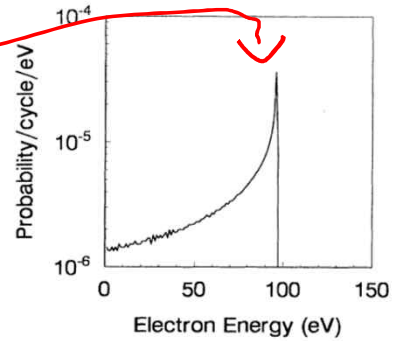

FIG. 1. Velocity distribution for electrons at the time of their first encounter with the ion. The parameters used for this calculation were those of helium with light intensity of 5×10^{14} W/cm^2 and wavelength 0.8 μm. The sharp cutoff in the electron energy occurs at $3.17U_p$.

Cutoff : 3 Up + Ip

Cited ~8000 times

Odd harmonics due to inversion symmetry

- Time domain

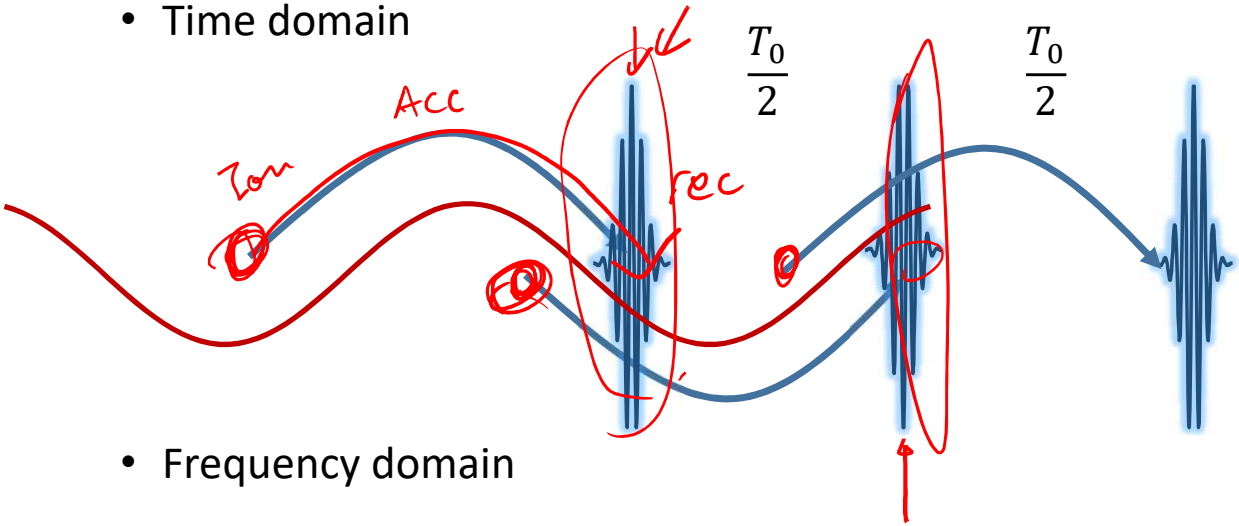

$$E_{XUV} = \sum_{m} E_{XUV}\left(t - \frac{mT_0}{2}\right)$$

- Frequency domain

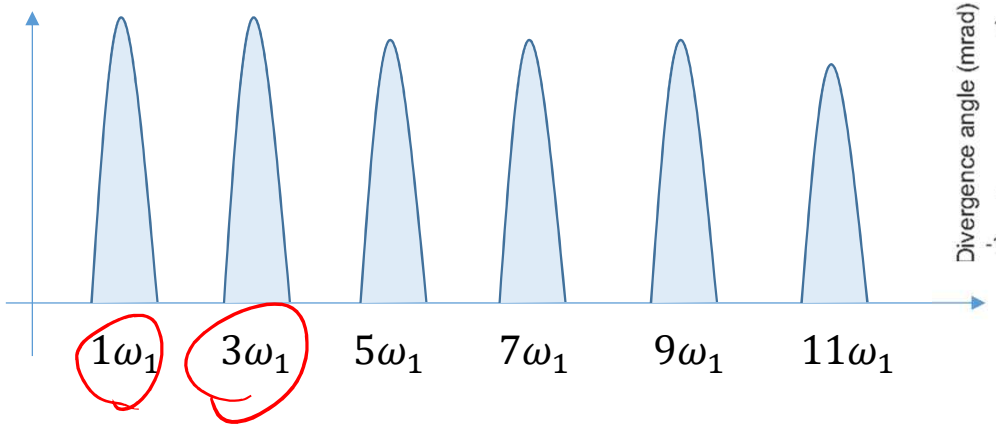

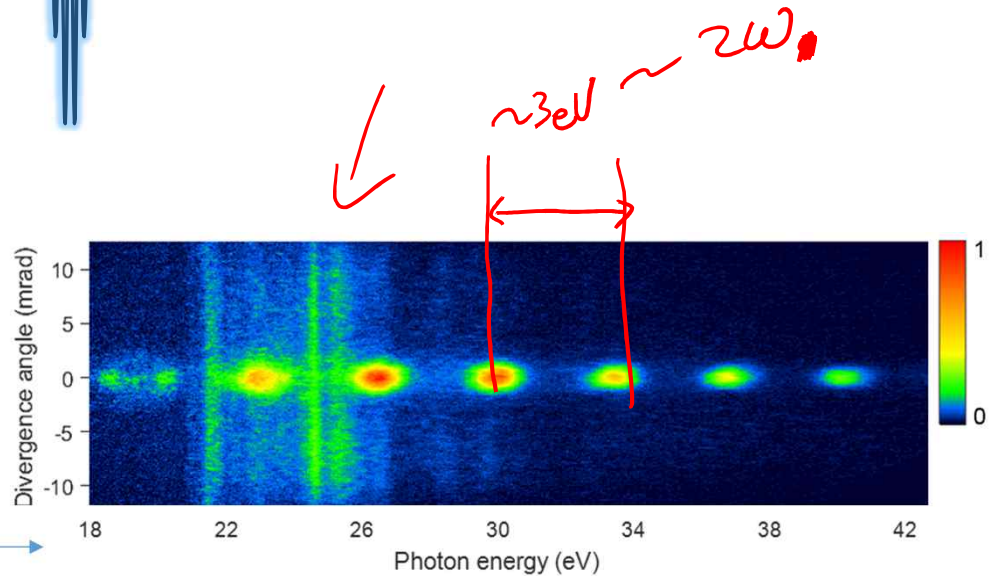

Intrinsic chirp of attosecond pulses

- Kinetic energy vs recombination time

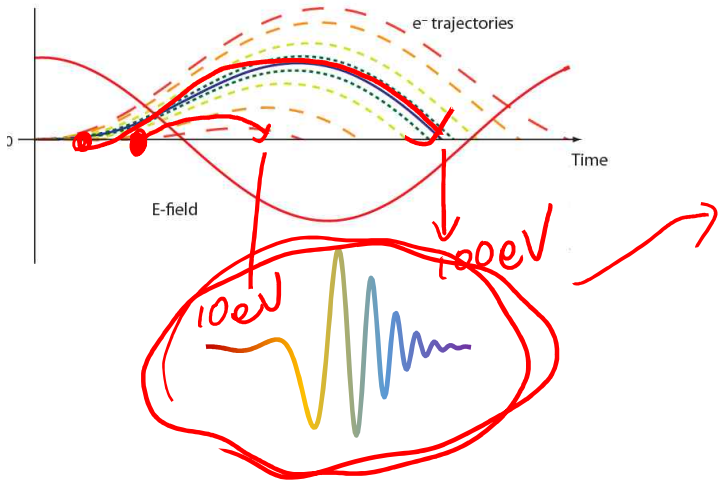

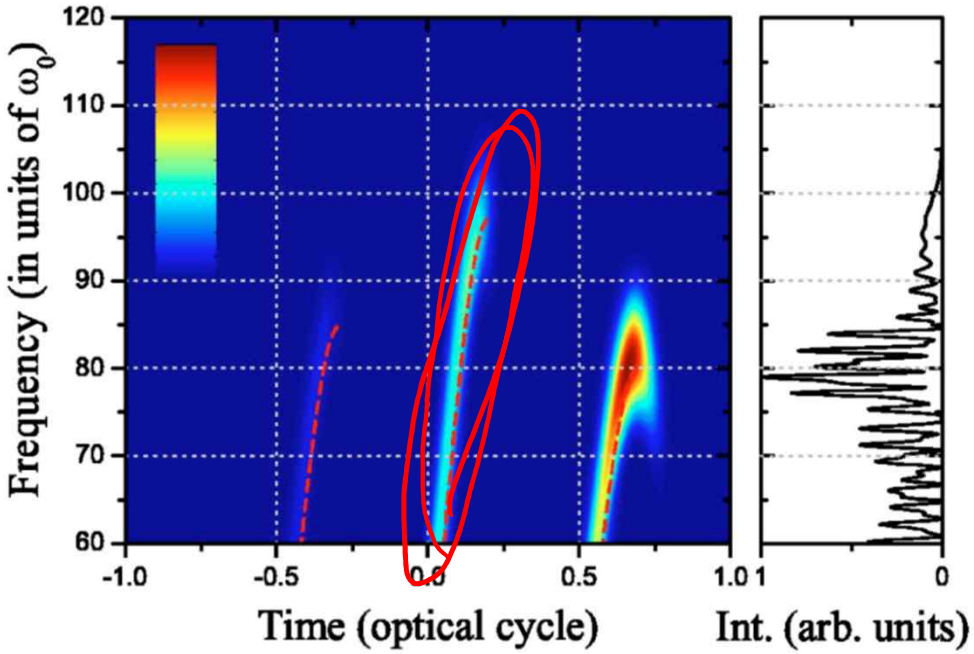

- Attosecond pulse is positively chirped.
- The intrinsic chirp of the attosecond pulse can compensated using x-ray fileters.

K. T. Kim et al., PRA **69**, 051850 (2004).

Attosecond pulse compression

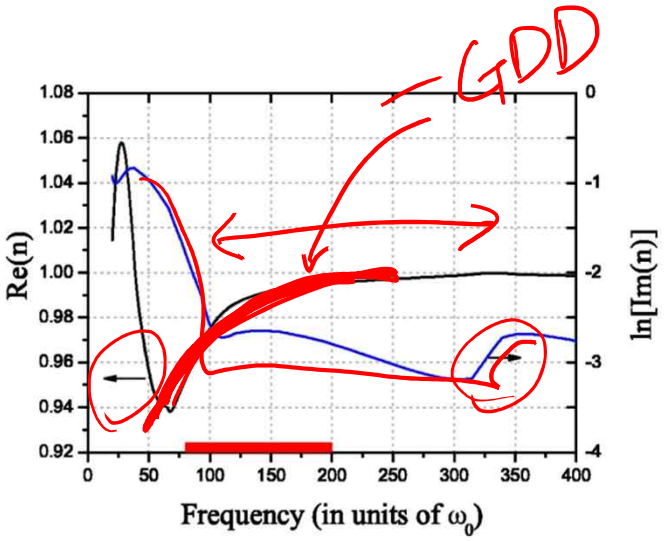

FIG. 2. (Color online) Real and imaginary parts of the refractive index of a Sn filter. The spectral range of negative GDD is marked as a thick red line.

They are related by the Kramers-Kronig relation so that the real part of the refractive index can be calculated from the photoabsorption data [14].

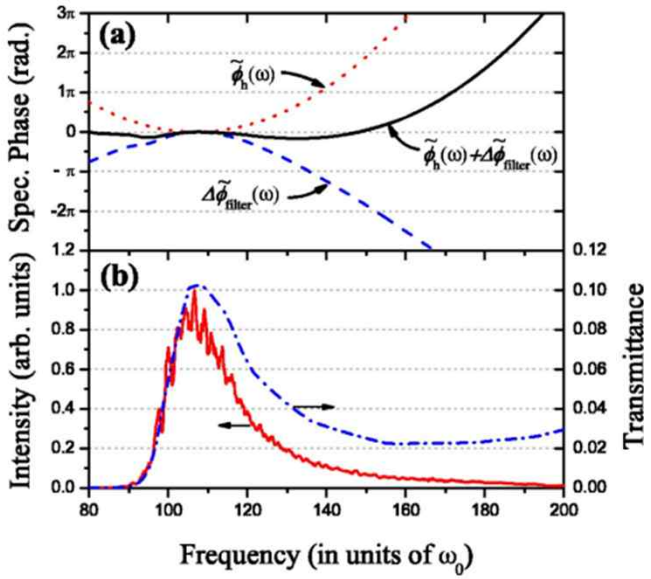

FIG. 3. (Color online) (a) Chirp compensation of positively chirped harmonic radiation by a Sn x-ray filter. The spectral phase of the harmonic radiation with a positive linear chirp centered at $107\omega_0$, $\tilde{\phi}_h(\omega)$, and the spectral phase shift induced by a 700-nm-thick Sn filter, $\Delta\tilde{\phi}_{\text{filter}}(\omega)$, are shown, respectively, by dotted and dashed lines. The spectral phase of the harmonic radiation after the Sn filter is shown as the solid line. (b) Spectral intensity of the harmonic radiation corresponding to Fig. 1(a), transmitted through the Sn filter (solid line) and the transmittance of the Sn filter (dash-dotted line).

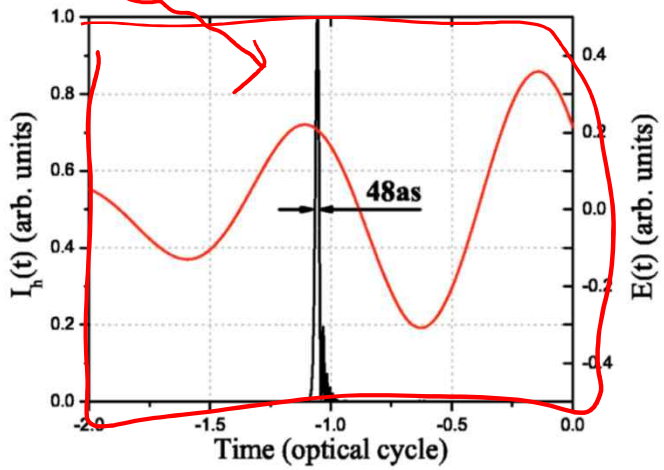

FIG. 4. (Color online) Temporal profile of the chirp-compensated attosecond pulse in the 700-nm Sn x-ray filter is shown along with the electric field of the 5-fs driving laser pulse.

K. T. Kim et al., PRA 69, 051850 (2004).

Single isolated attosecond pulse generation

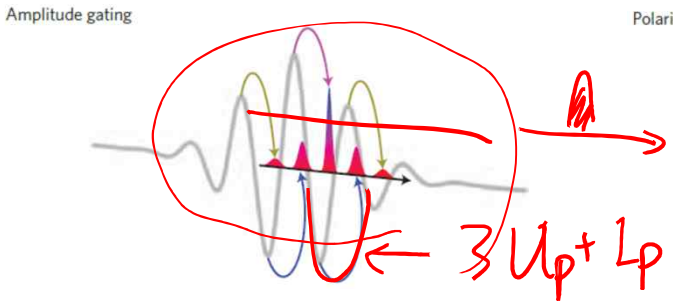

R. Kienberger et al., Nature **427**, 817 (2004)

G. Sansone et al., Science **314**, 443 (2006)

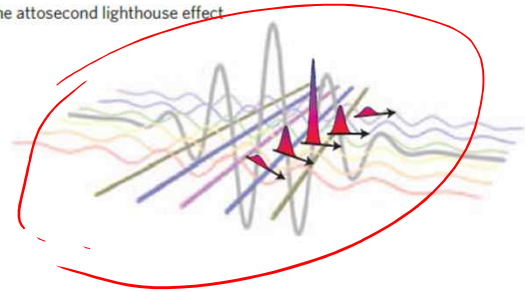

K. T. Kim et al., Nat Phonics **7**, 651 (2013)

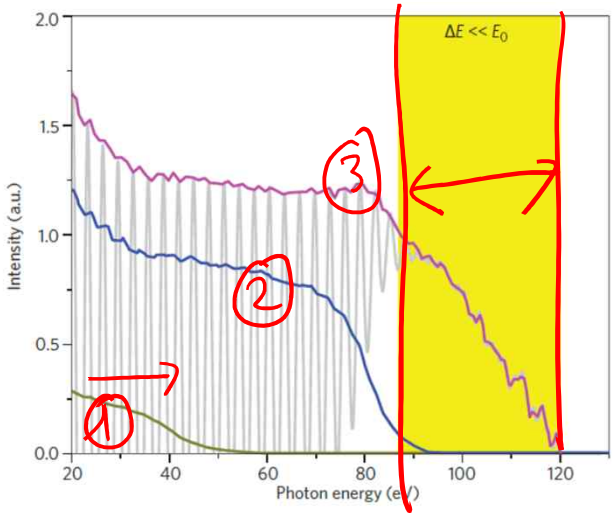

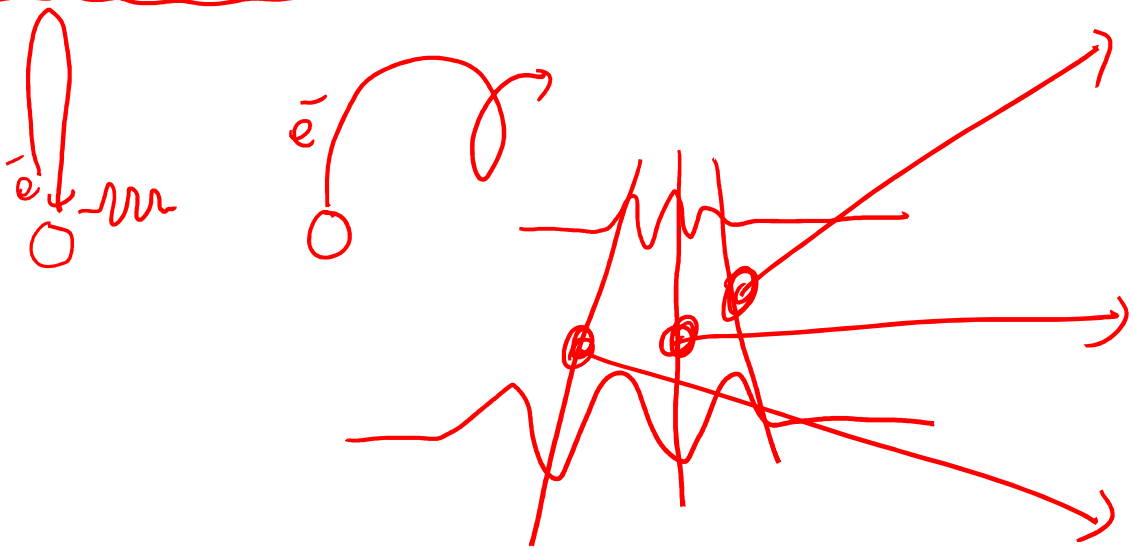

Attosecond pulse characterization

- RABBITT (reconstruction of attosecond beating by interference of two-photon transitions)

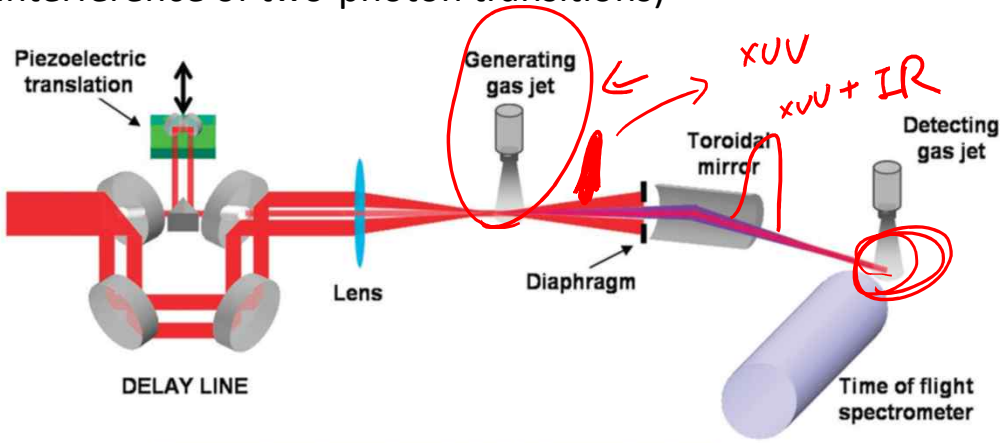

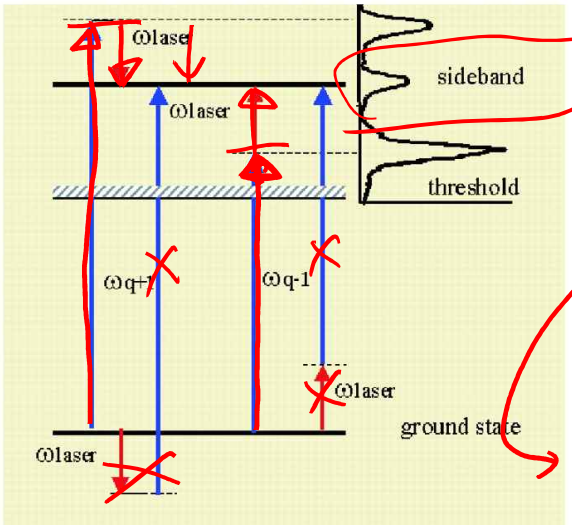

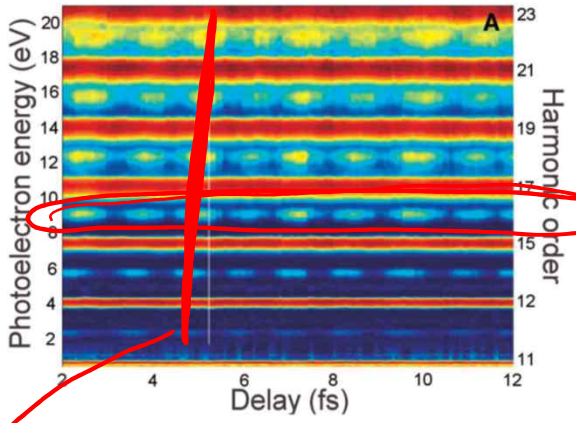

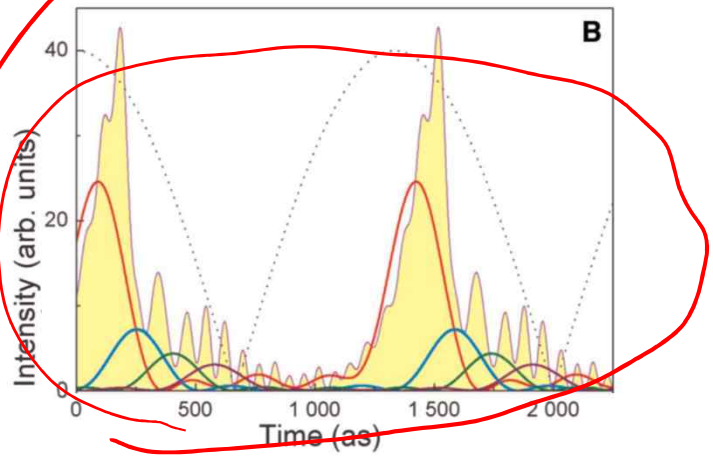

$$A_f \cos(2\varphi_{IR} + \varphi_{q-1} - \varphi_{q+1} + \Delta\varphi_{atomic}^{f})$$

P. M. Paul et al., Science **292**, 1689 (2001)
Y. Mairesse et al., Science **302**, 1540 (2003)

Attosecond pulse characterization (attosecond streaking)

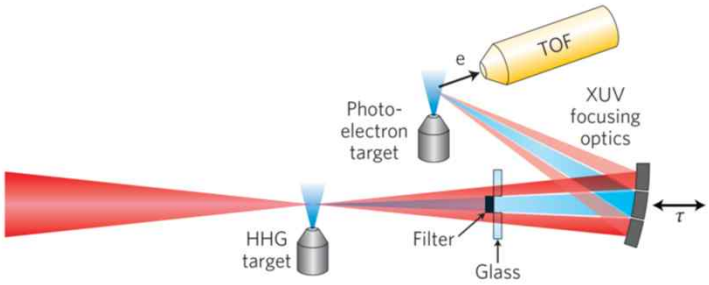

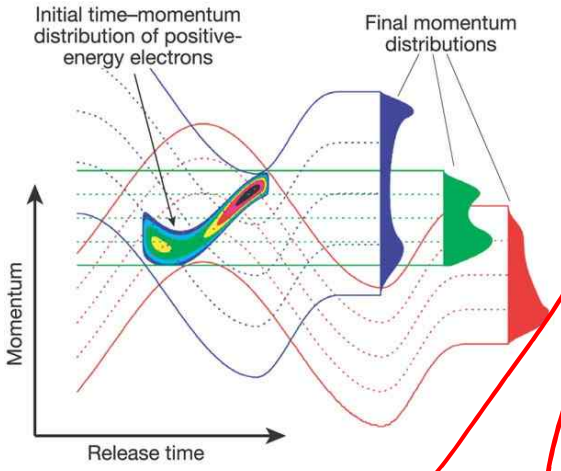

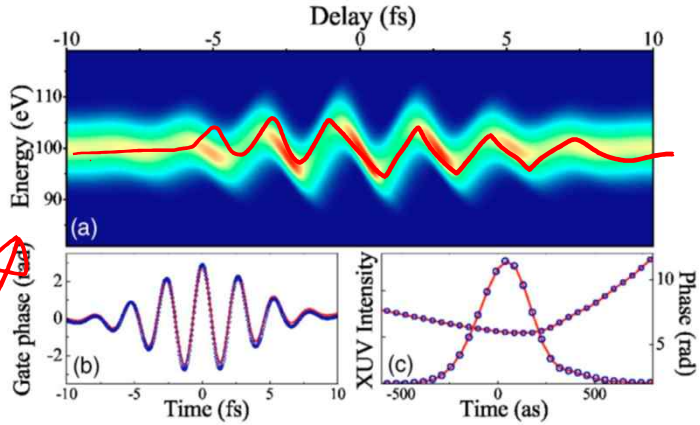

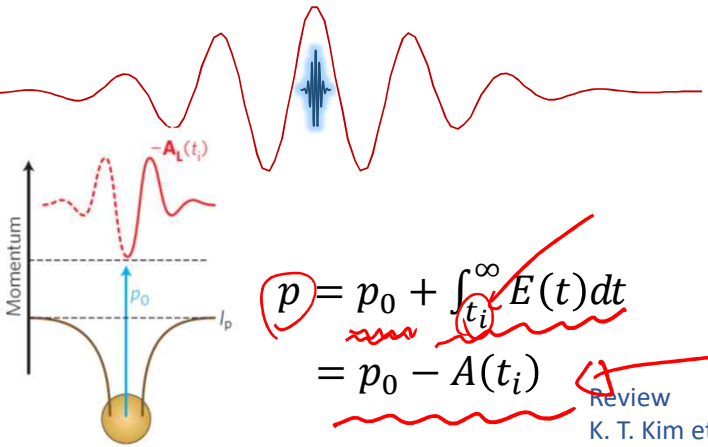

$$p = p_0 + \int_{t_i}^{\infty} E(t)dt$$
$$= p_0 - A(t_i)$$

Review
K. T. Kim et al., Nat. Photonics **8**, 187 (2014)

Atomic transient recorder
R. Kienberger et al., Nature **428**, 817 (2004)

Y. Mairesse et al., Phys. Rev. A **71**, 011401(2005)

Frequency resolved optical gating for attosecond pulses

Transition amplitude (ground -> continuum)

$$a(\mathbf{v},\tau) = -i\int_{-\infty}^{+\infty} dt e^{i\phi(t)}\mathbf{d}_{\mathbf{p}(t)}E_X(t-\tau)e^{i(W+Ip)t},$$

$$\phi(t) = -\int_{t}^{+\infty} dt'[\mathbf{v}\cdot\mathbf{A}(t') + \mathbf{A}^2(t')/2].$$

FROG

$$S(\omega,\tau) = \left|\int_{-\infty}^{+\infty} dt G(t)E(t-\tau)e^{i\omega t}\right|^2$$

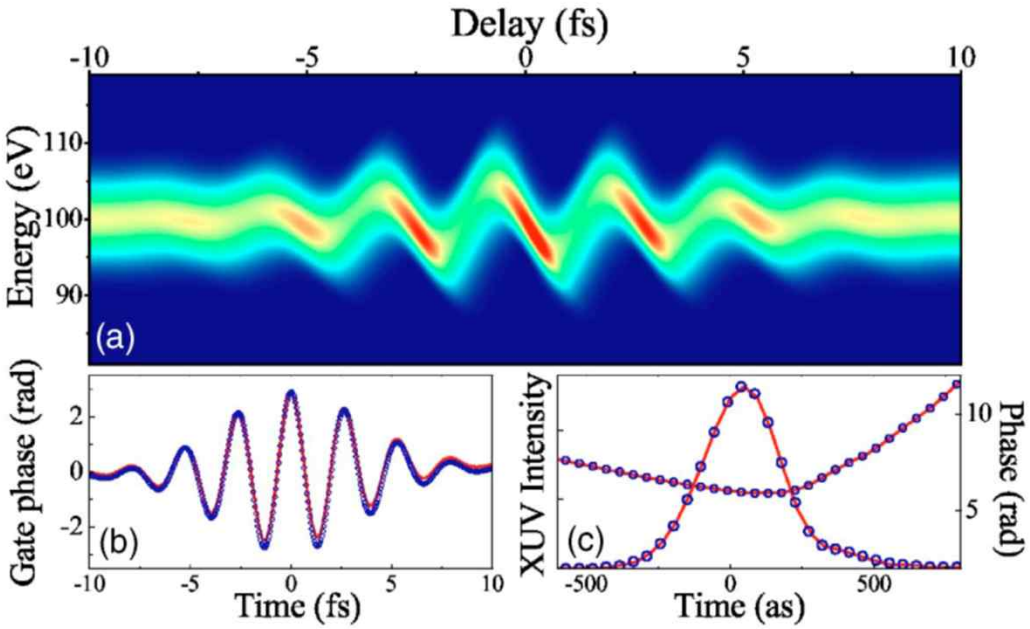

Frequency-resolved optical gating for complete reconstruction of attosecond bursts
Y. Mairesse et al., Phys. Rev. A **71**, 011401(2005)

Kicking a ball over a potential valley

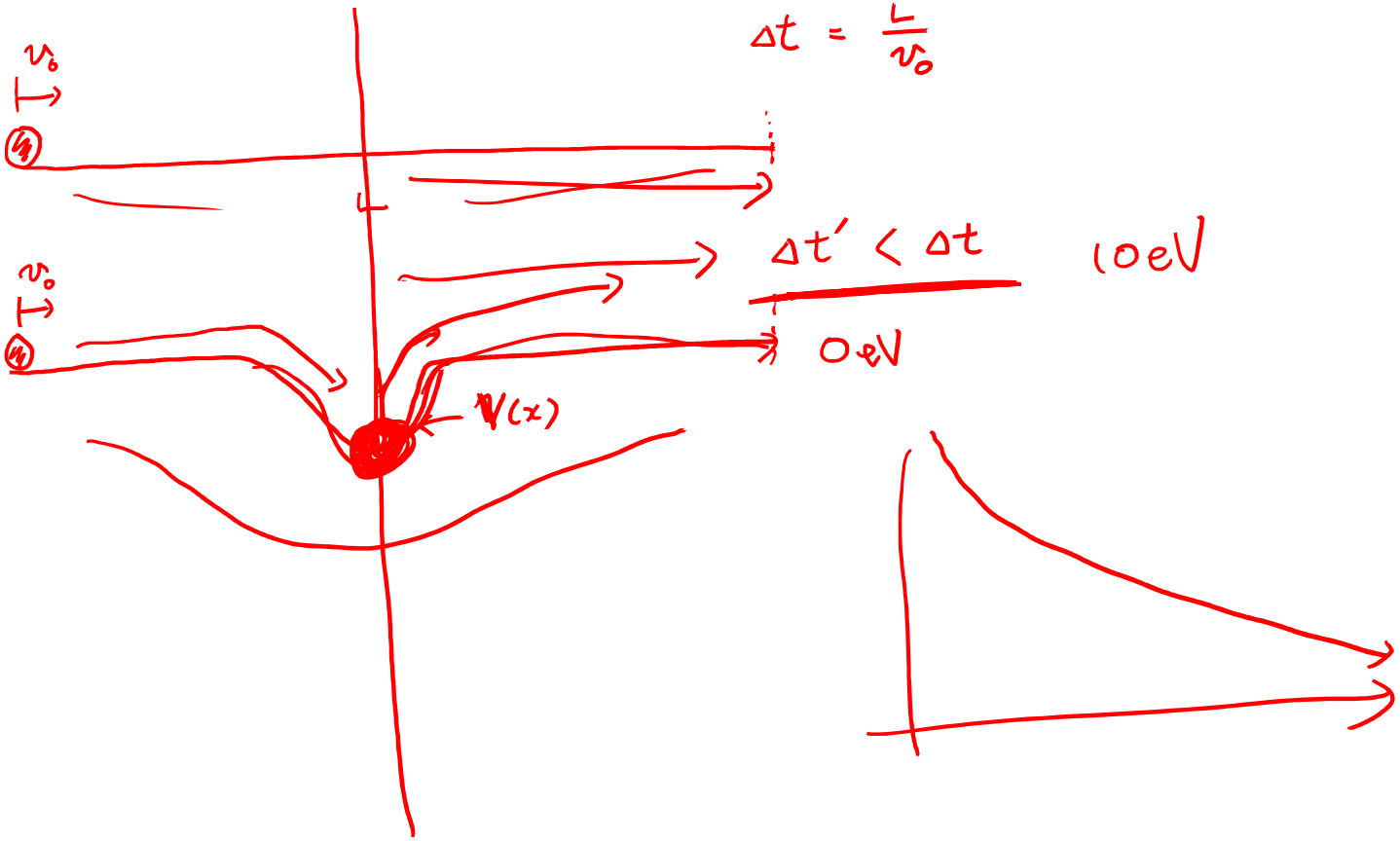

Delay in photoionization

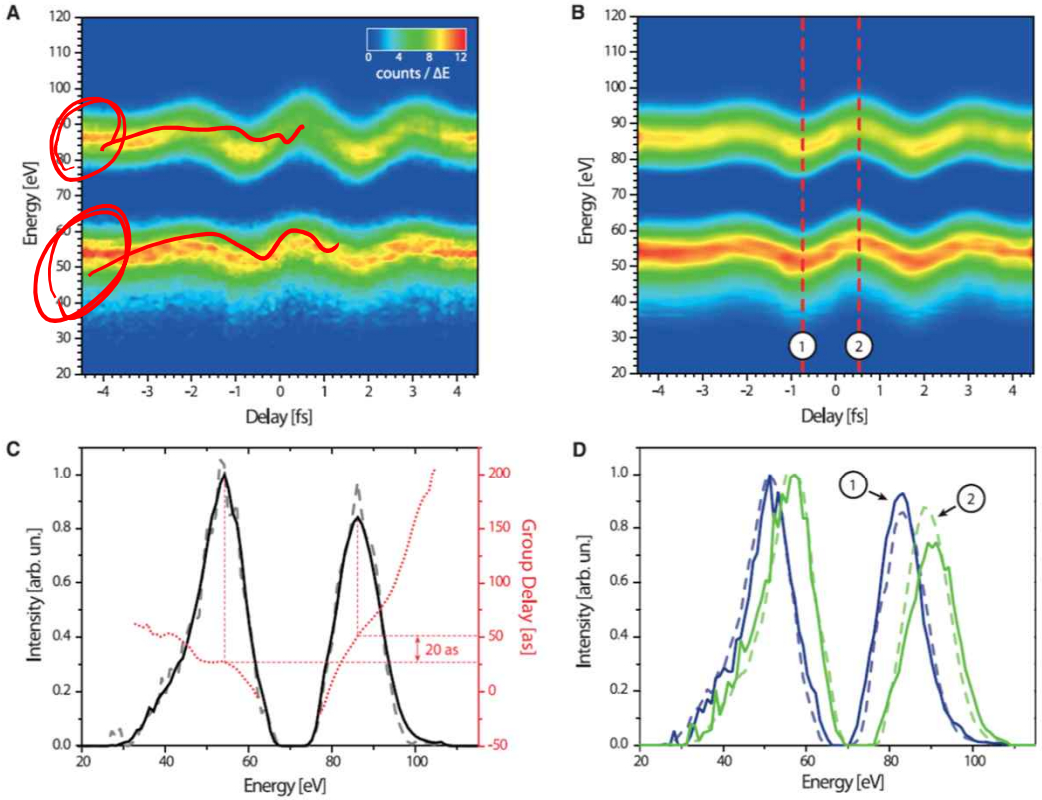

Fig. 2. Attosecond streaking spectrograms (**A** and **B**), evaluated photoelectron wave packets (**C**), and streaked spectra (**D**). The spectrograms in (A) are composed of a series of photoelectron energy spectra recorded by releasing 2*s* and 2*p* electrons from Ne with an attosecond XUV pulse in the presence of a strong NIR few-cycle laser field, as a function of the delay between the XUV and NIR fields. The spectrogram is processed with a FROG algorithm tailored for streaking measurements (*30*). (B) shows the spectrogram reconstructed by this algorithm. The retrieved 2*s* and 2*p* spectra, together with the respective group delays, are plotted in (C) (black solid line and red dotted line, respectively). The reconstructed energy spectra are in excellent agreement with the measured ones (gray dashed line). The average difference between the group delays corresponds to a 20-as retardation of the 2*p* emission with respect to the 2*s* emission. (D) compares reconstructed and measured streaked spectra at two delays, which exhibit the largest positive and negative shifts of the electron energy distribution.

Wigner Smith time delay

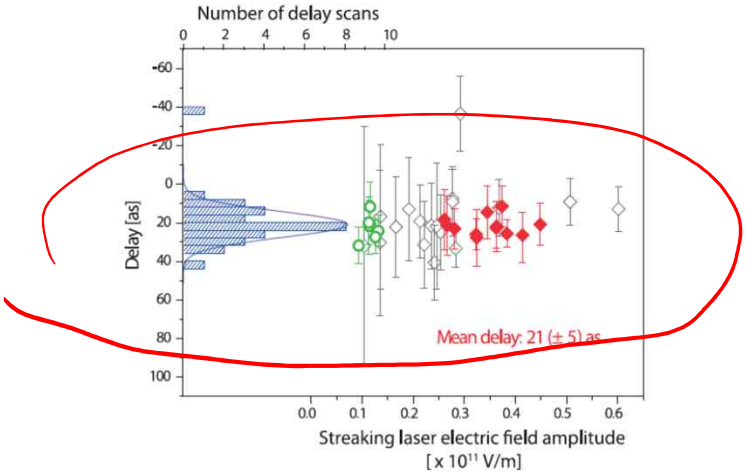

Fig. 3. The relative delay between photoemission from the 2*p* and 2*s* subshells of Ne atoms, induced by sub–200-as, near–100-eV XUV pulses. The depicted delays are extracted from measured attosecond streaking spectrograms by fitting a spectrogram, within the strong-field approximation, with parameterized NIR and XUV fields. Our optimization procedure matches the first derivatives along the time delay dimension of the measured and reconstructed spectrograms, thereby eliminating the influence of unstreaked background electrons [for details on the fitting algorithm, see (*29*)]. From the analysis of a set of spectrograms, the measured delays and associated retrieval uncertainties are plotted against the amplitude of the vector potential applied in the attosecond streak camera. Spectrograms measured in the presence of a satellite attosecond pulse were found to exhibit a less accurate retrieval of the delay value. When a subset of data (red diamonds) that represents scans with less than 3% satellite pulse content was evaluated, a mean delay value of 21 as with a standard deviation of ~5 as was found. The green circles represent the result of analyzing spectrograms recorded with an XUV pulse with narrower bandwidth in order to exclude the potential influence of shakeup states contributing to the electron kinetic energy spectrum.

M. Schultze et al., Science 328, 1658 (2010)

High harmonic generation (quantum mechanical description)

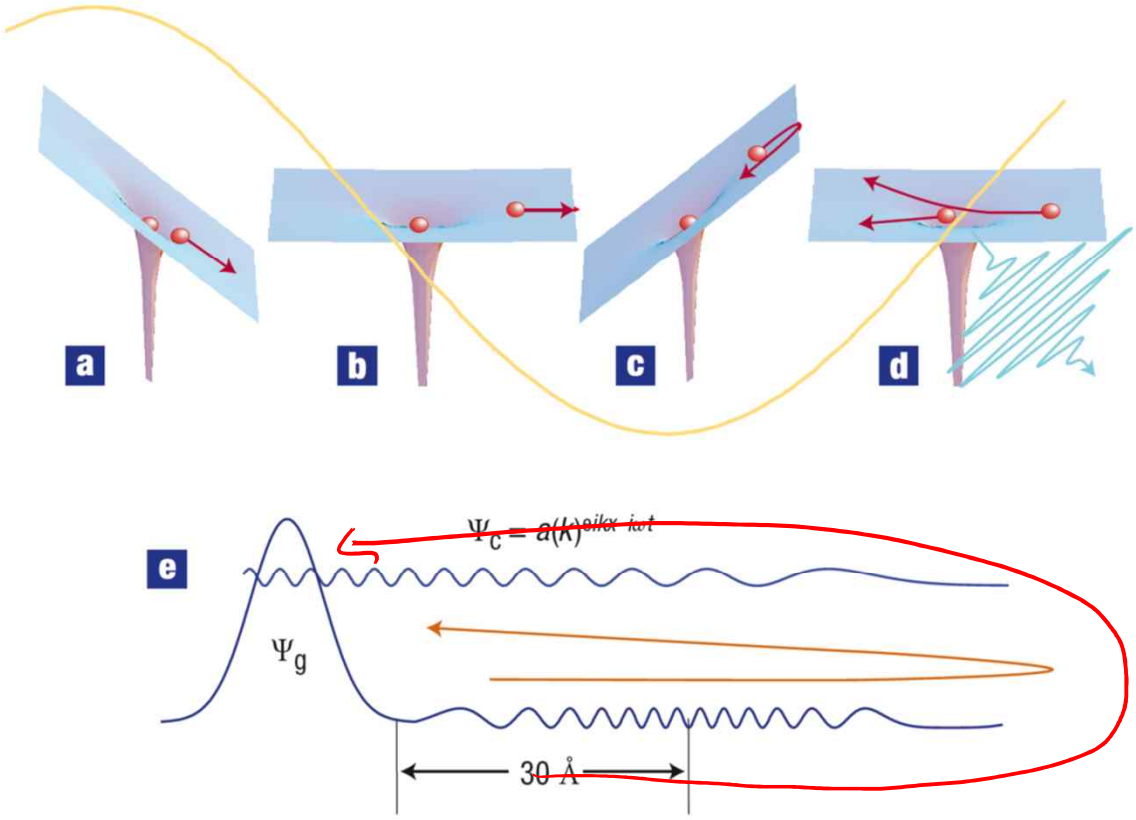

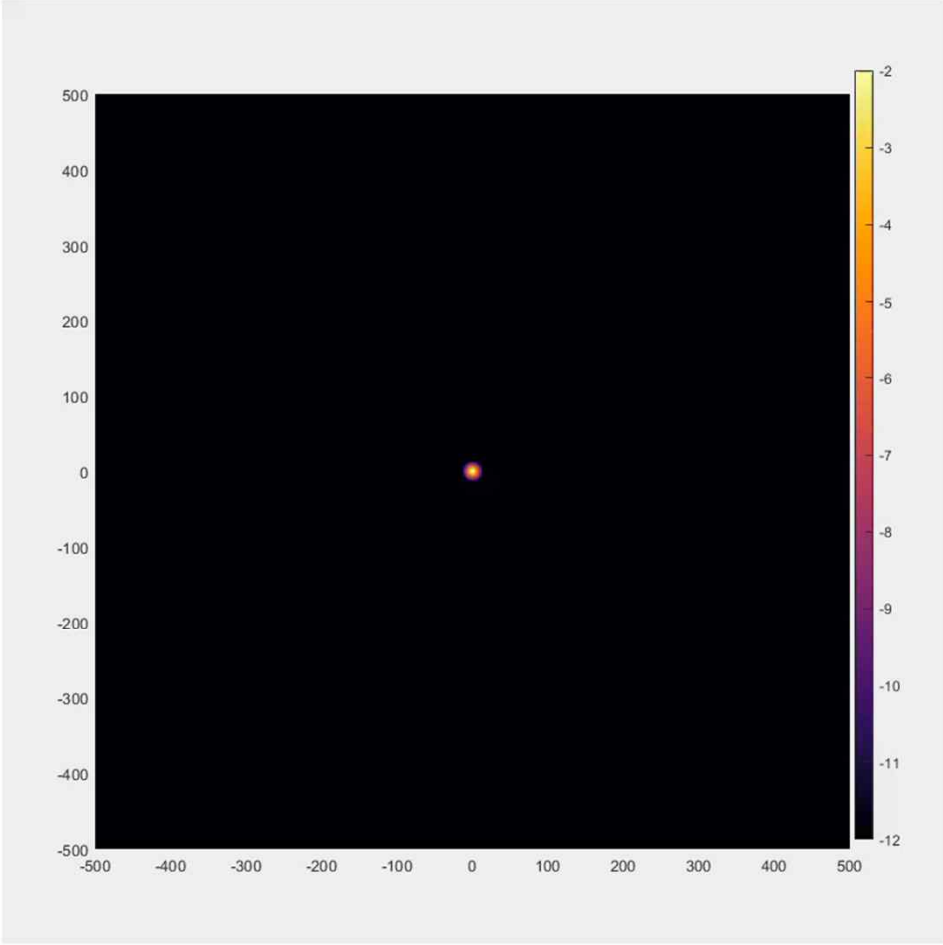

Quantum interference during high-order harmonic generation from aligned molecules

HHG is enhanced when ionization is enhanced
Ionization and HHG correlated

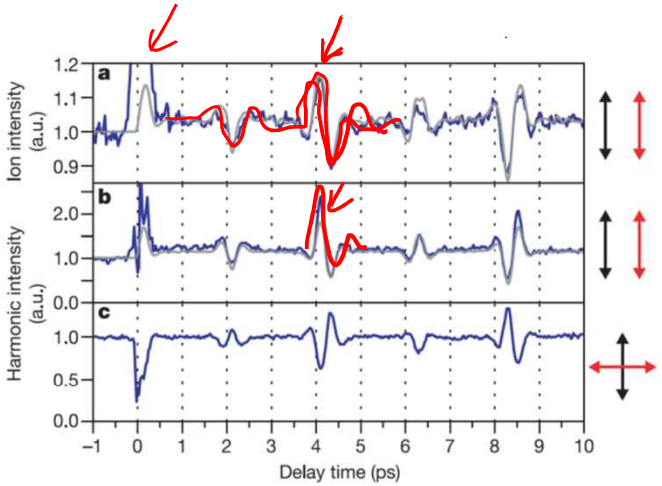

Figure 1 | The time evolution of the ion yield and the 23rd harmonic intensity from N_2 molecules. **a–c**, The ion yield dominated by N_2^+ (**a**) and the 23rd harmonics from N_2 molecules (**b**, **c**) as a function of pump–probe delay. The polarizations of the pump (black arrow) and the probe (red arrow) pulses are parallel (**a**, **b**) or perpendicular (**c**) to each other. Note that the rotational period T_{rot} of a N_2 molecule is 8.4 ps. The results of theoretical calculations are shown by grey curves. The rotational temperature of the N_2 molecules is assumed to be 80 K, and the highest degree of alignment $\langle\cos^2\theta\rangle$ is estimated to be 0.62 at $T_{rot}/2$. a.u., arbitrary units.

T_{rot} (~8.4 ps) σ_g symmetry

Ionization and HHG anti correlated

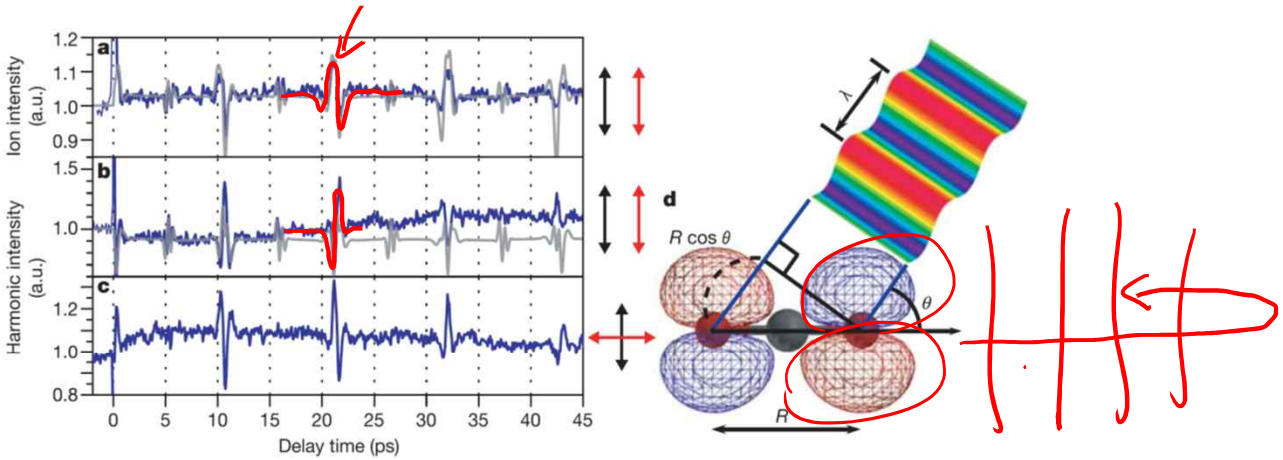

Figure 3 | The time evolution of the ion yield and the 23rd harmonic intensity from CO_2 molecules, and an illustration of the model of two point emitters. **a–c**, The ion yield dominated by CO_2^+ (**a**) and the 23rd harmonics from CO_2 molecules (**b**, **c**) as a function of pump–probe delay. The experimental conditions are identical with those of Fig. 1. Note that the rotational period T_{rot} of a CO_2 molecule is 42.7 ps. The results of theoretical calculations are shown by grey curves. The rotational temperature of CO_2 molecules is assumed to be 40 K, and the highest degree of alignment $\langle\cos^2\theta\rangle$ is estimated to be 0.70 at $3T_{rot}/4$. **d**, A CO_2 molecule can be regarded as an appropriately elongated diatomic molecule. Two point emitters are located in two O nuclei depicted as red spheres. λ is the de Broglie wavelength of a free electron. θ is the orientation angle, that is, the angle between the molecular axis and the polarization direction of the probe pulse. R and $R\cos\theta$ are the distance between two O atoms and its projection, respectively. In the recombination process, the destructive or constructive interference takes place depending on the conditions (equations (2) and (3)) given in the text.

anti-bonding π_g symmetry

T. Kanai et al., Nature **435**, 470 (2005)

Tomographic imaging of molecular orbitals

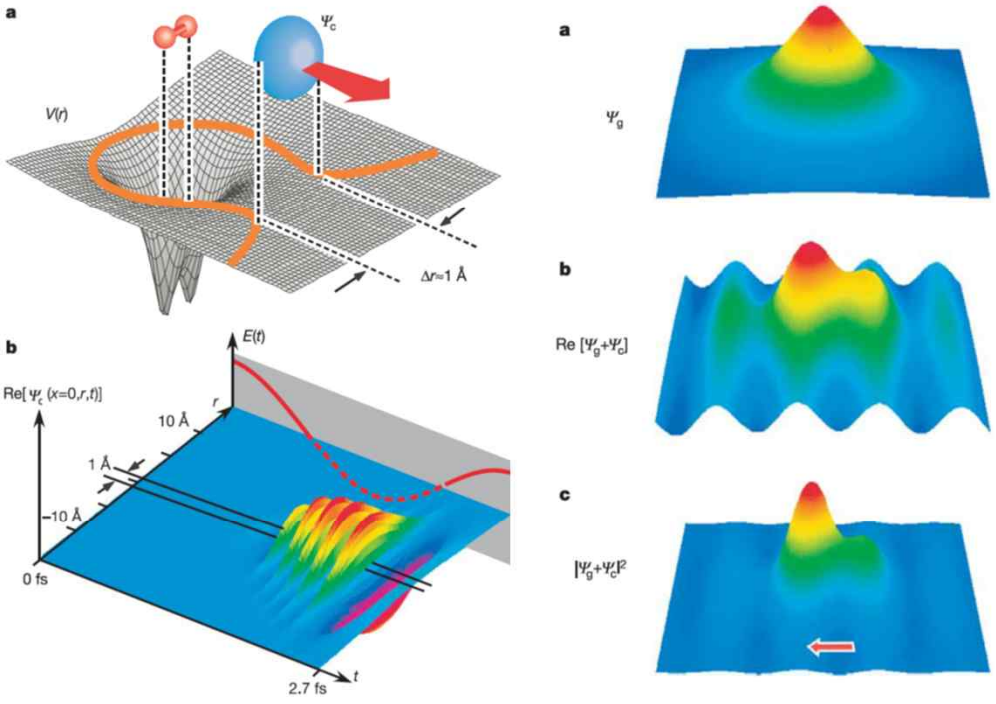

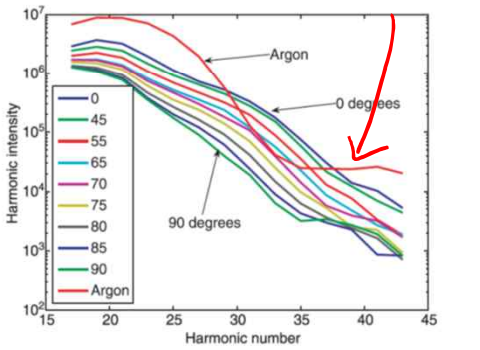

Figure 3 High harmonic spectra were recorded for N_2 molecules aligned at 19 different angles between 0 and 90° relative to the polarization axis of the laser. For clarity, only some of the angles have been plotted above. The high harmonic spectrum from argon is also shown; argon is used as the reference atom. Clearly the spectra depend on both the alignment angle and shape of the molecular orbital.

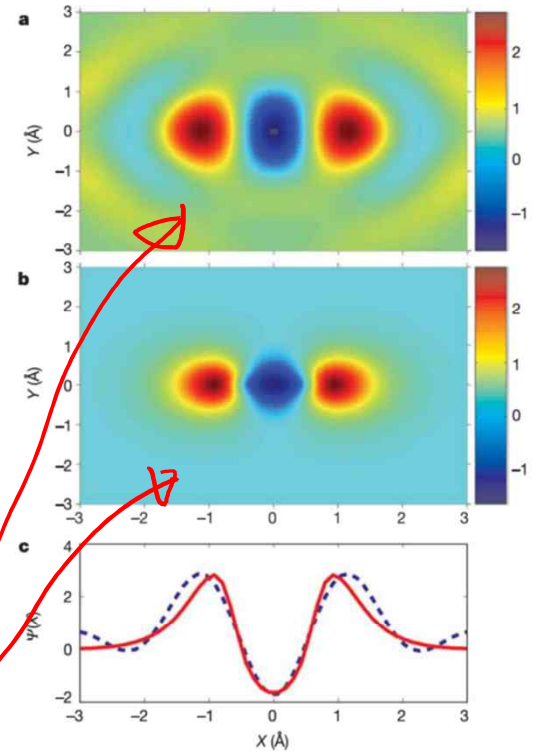

Figure 4 Molecular orbital wavefunction of N_2. **a**, Reconstructed wavefunction of the HOMO of N_2. The reconstruction is from a tomographic inversion of the high harmonic spectra taken at 19 projection angles. Both positive and negative values are present, so this is a wavefunction, not the square of the wavefunction, up to an arbitrary phase. **b**, The shape of the N_2 $2p\,\sigma_g$ orbital from an *ab initio* calculation. The colour scales are the same for both images. **c**, Cuts along the internuclear axis for the reconstructed (dashed) and *ab initio* (solid) wavefunctions.

J. Itatani et al., Nature **432**, 867 (2004)

Following a chemical reaction using high-harmonic interferometry

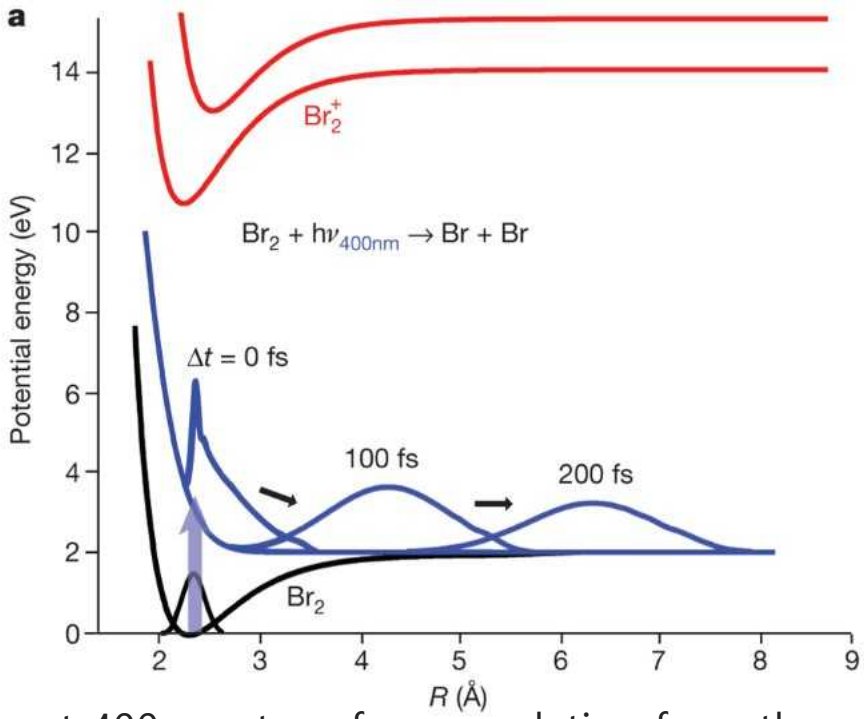

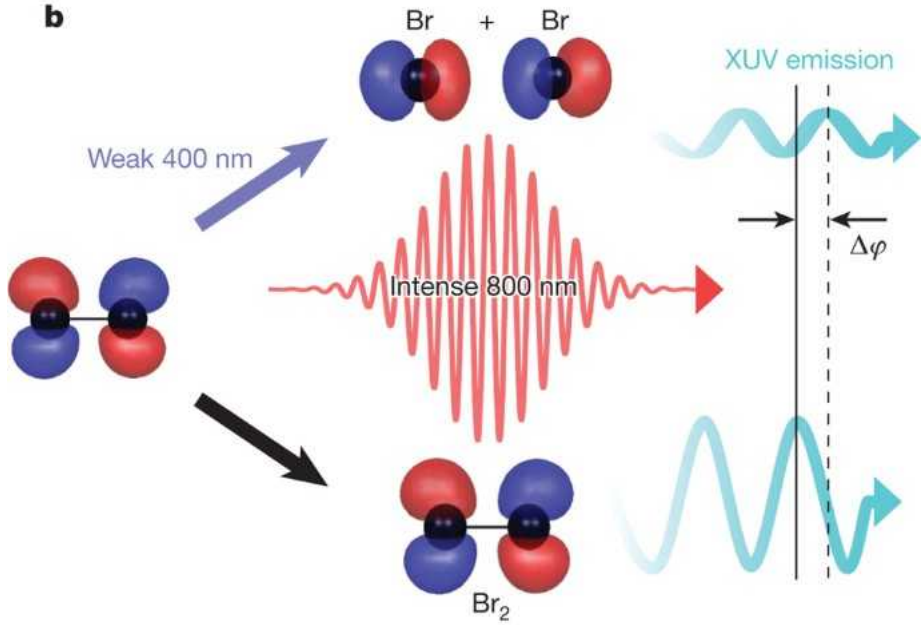

Excitation at 400 nm transfers population from the X $^1\Sigma_g^+$ ground state to the repulsive C $^1\Pi_{1u}$ state in which it dissociates

H. J. Worner et al., Nature **466**, 604 (2010)

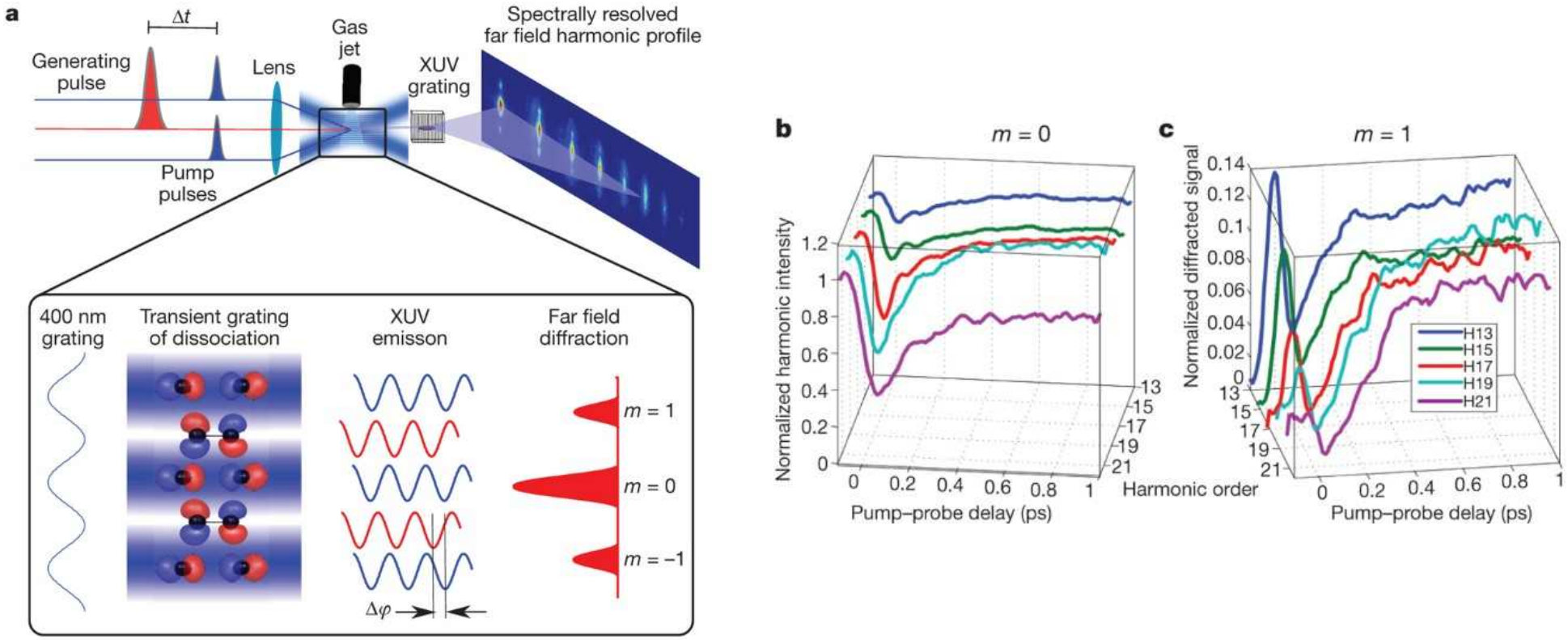

H. J. Worner et al., Nature **466**, 604 (2010)

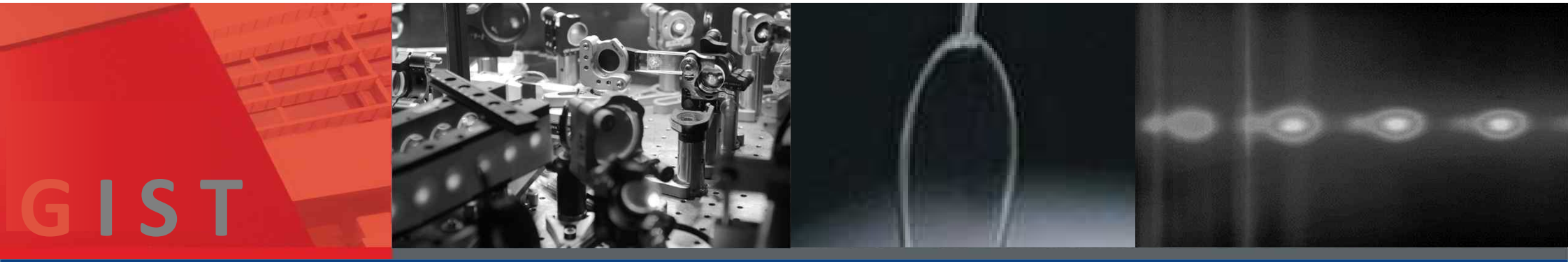

Frustrated tunneling ionization

Frustrated tunneling ionization

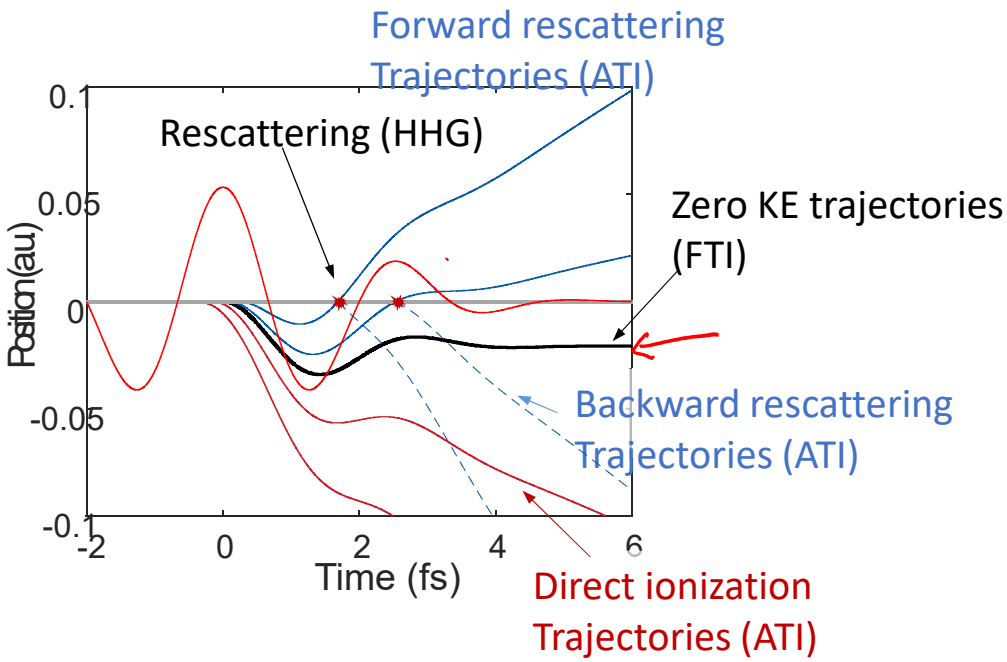

$I = 10^{15}$ W/cm^2

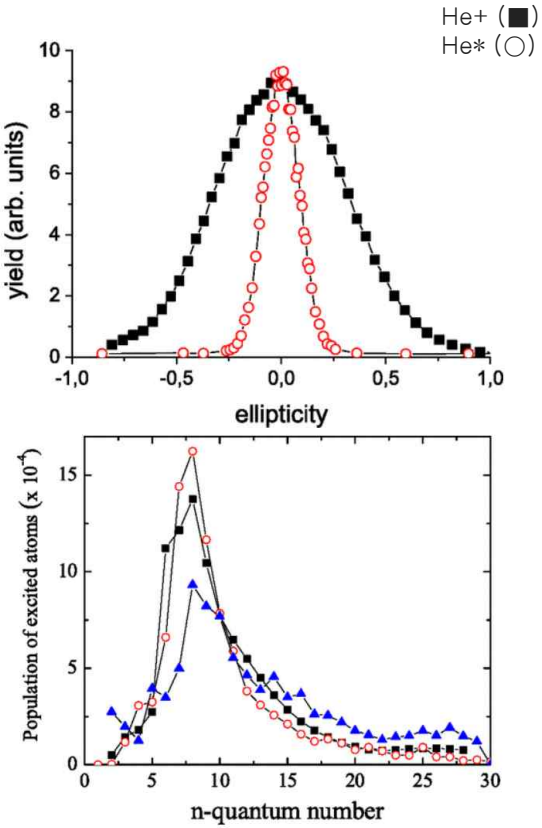

Motivation - observation of a strange EUV emission

What are these lines? Is this atomic line emission?

He HHG spectrum using a 5-fs pulse (linear pol)

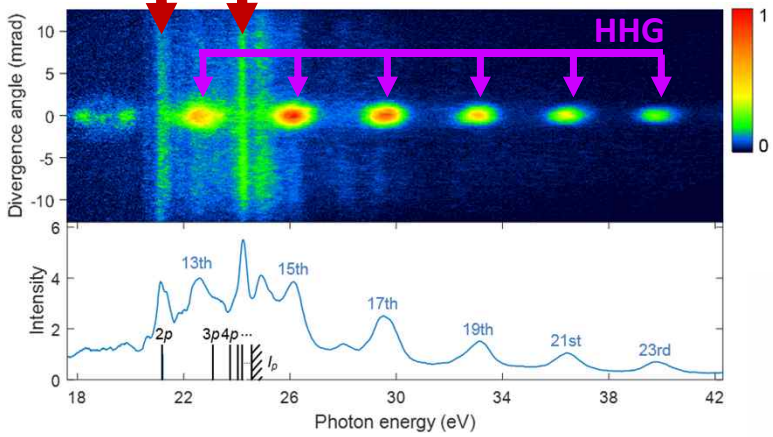

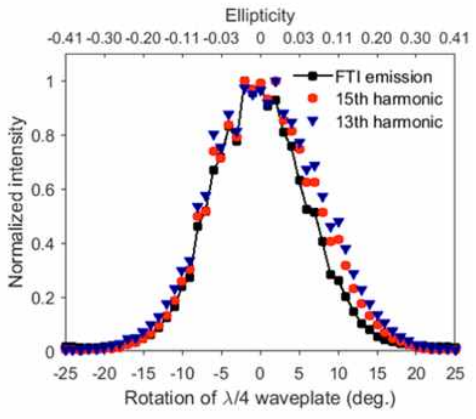

N_2 atomic line emission (circular pol)

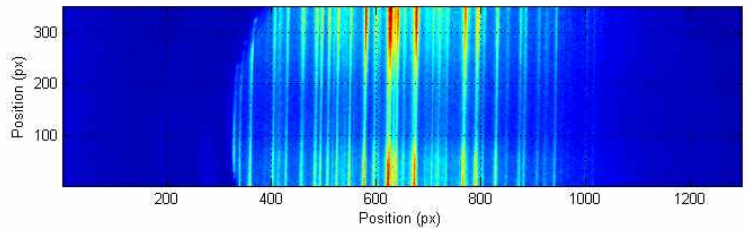

Comparison with NIST data

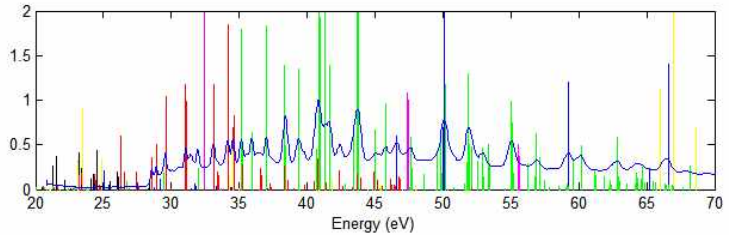

Atomic line emission can be clearly observed when **a circular pol** is used. Otherwise, HHG is too strong!

The intensity dependence on the ellipticity tells us that the process is related with recollision dynamics

High harmonic generation and frustrated tunneling ionization

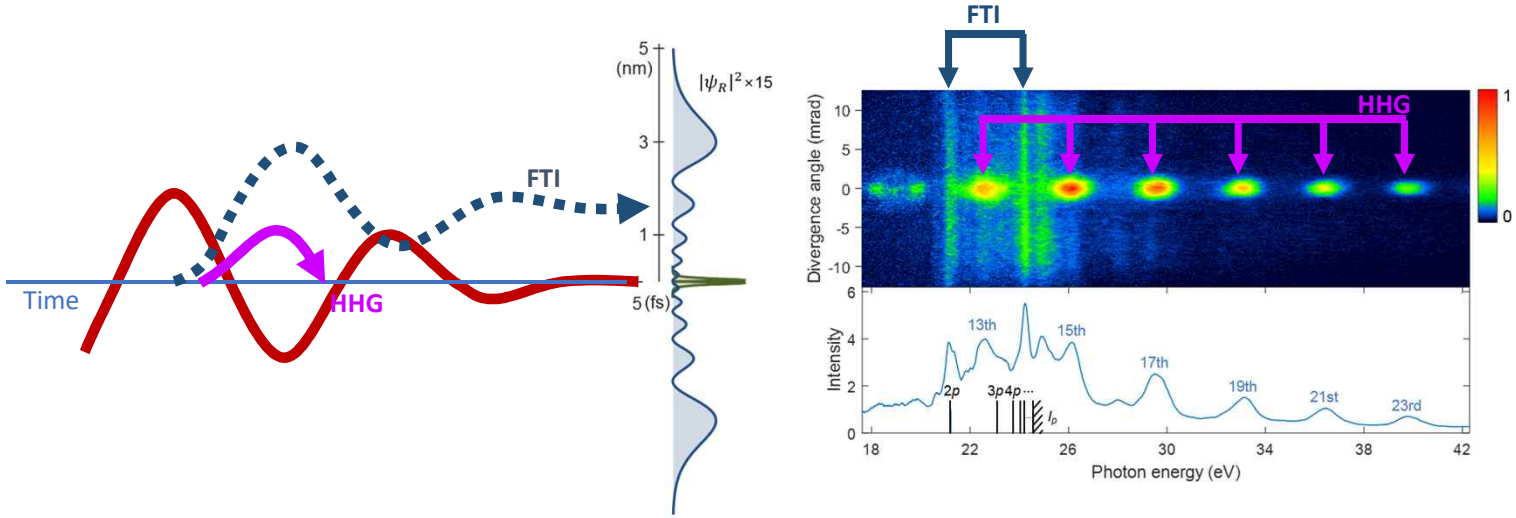

HHG (3 step): Ionization, Acceleration, Recombination
FTI (4 step): Ionization, Acceleration, Recombination, Free induction decay

Attosecond lighthouse experiment with FTI emission

Coherent control using attosecond lighthouse technique

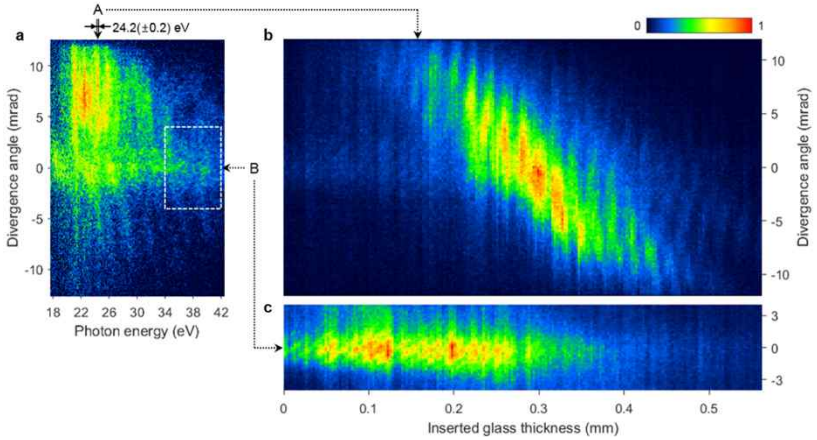

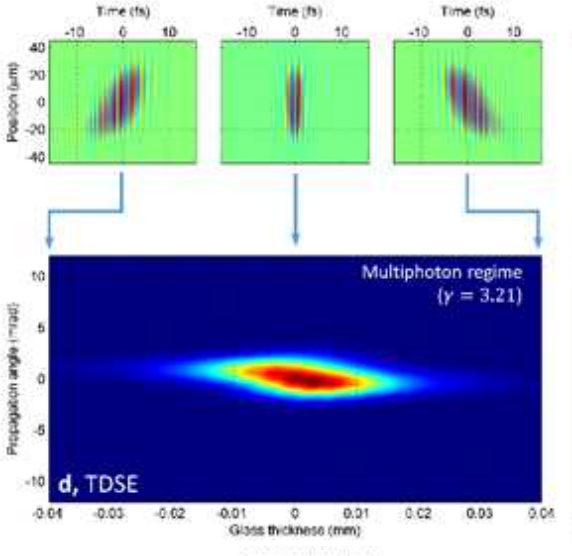

It is an FTI emission!
Not an atomic line emission after multi-photon absorption!

H. Yun *et al.*, "Coherent EUV emission through FTI", Nature Photonics **12**, 620-624 (2018).

Experiment setup for the generation of an FTI emission

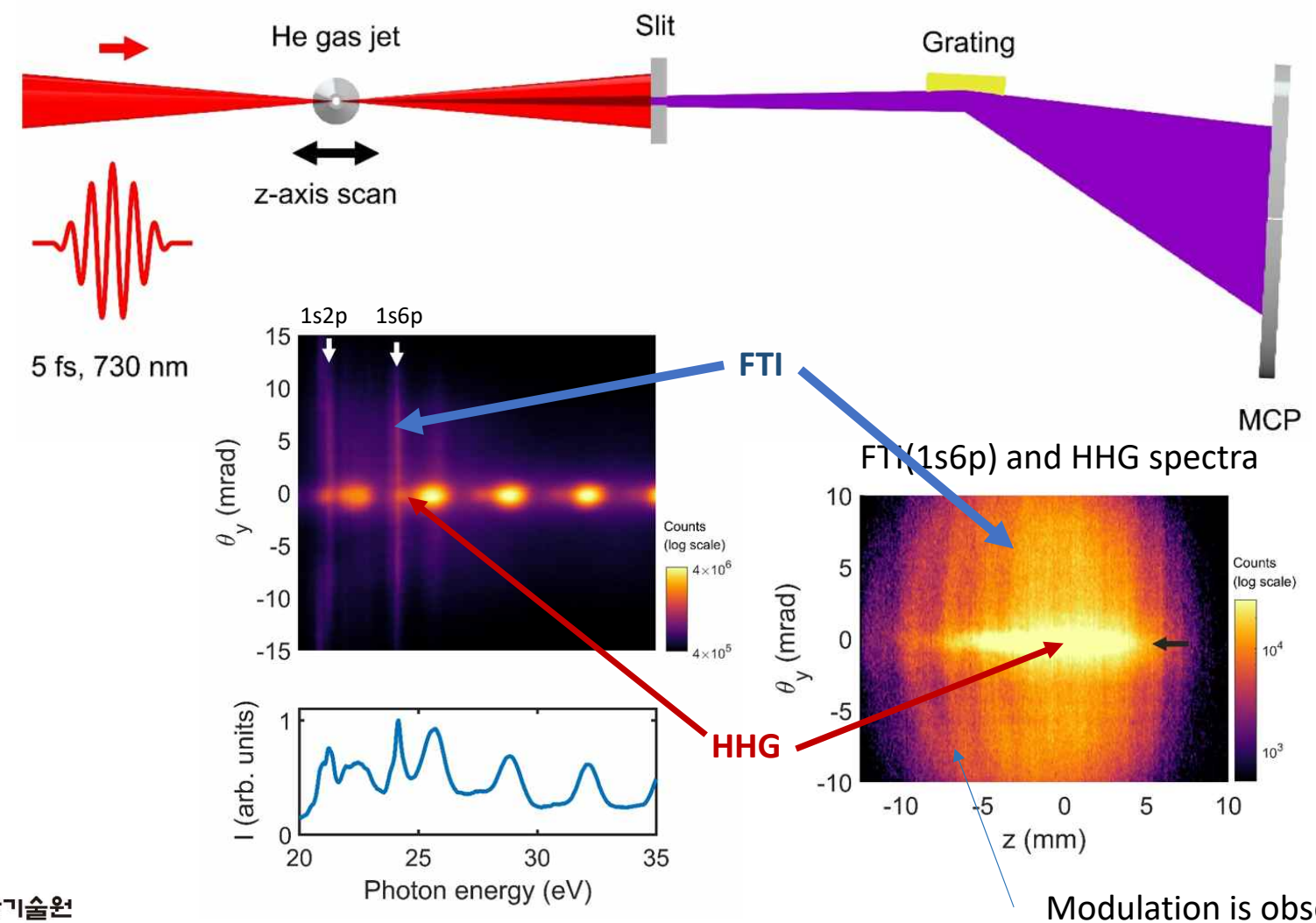

Coherent control of FTI emission

Phase of FTI emission vs position

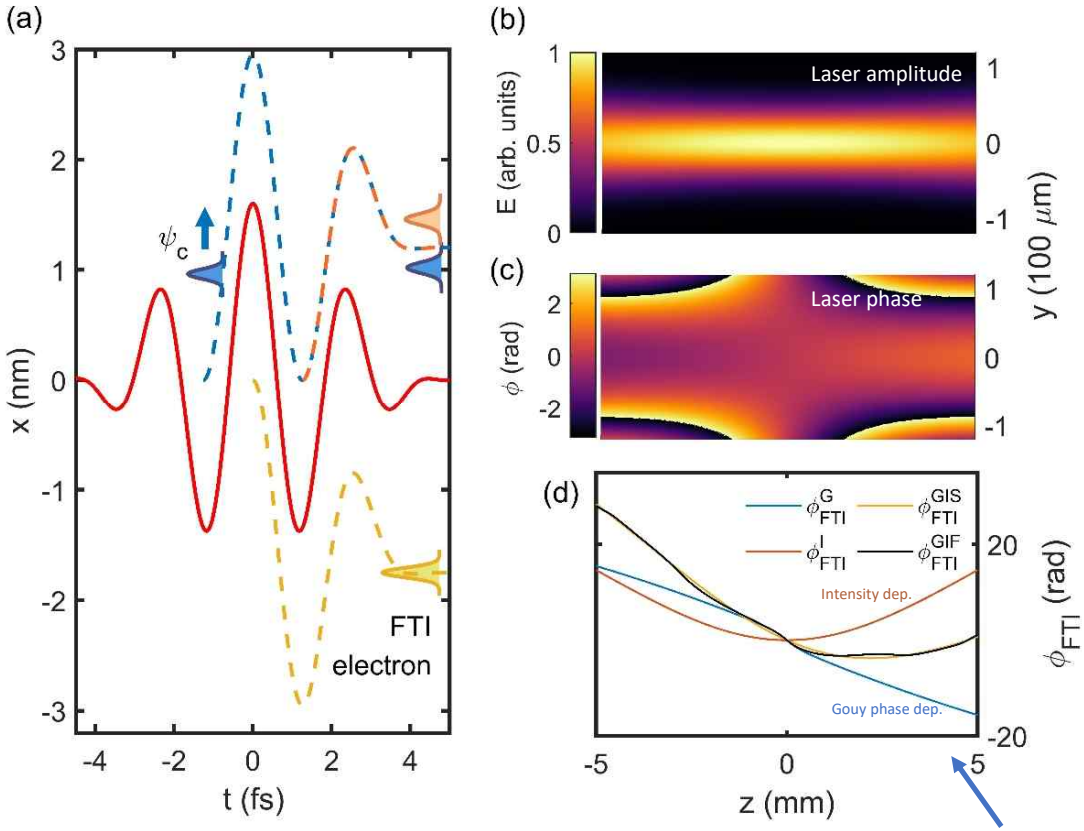

FTI HHG

Four step model

- Ionization,
- acceleration,
- Recombination to excited state,
- Emission through free induction decay

Strong field approximation

$$\Phi_{FTI} = I_P t_i - \int_{t_i}^{t_r} \frac{v^2}{2} dt$$

P. Salieres et al., PRL 74, 3776 (1995).

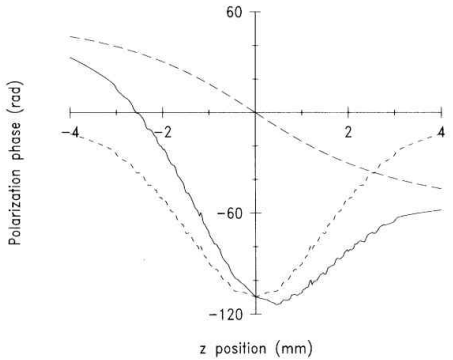

FIG. 2. Phase of the polarization on the propagation axis (solid line). The long-dashed line indicates the term due to the propagation of the fundamental, and the small-dashed line the dipole phase for a peak intensity $I_0 = 6 \times 10^{14}$ W/cm^2. The laser propagates from the left to the right.

FTI emission at different target positions

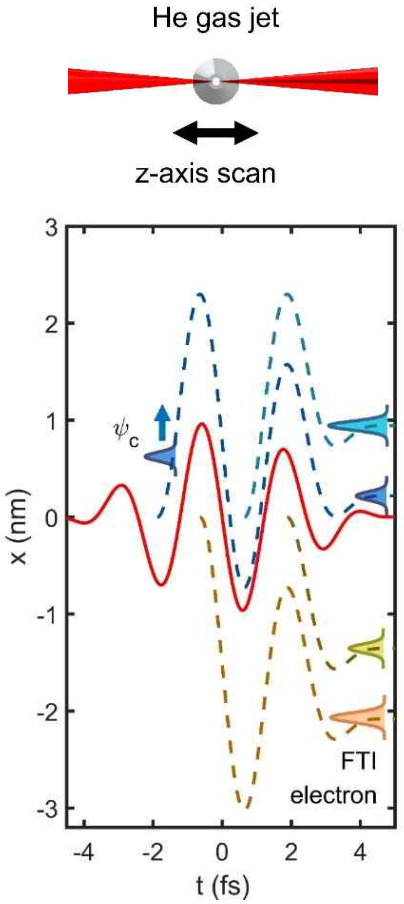

Experiments **Calculations**

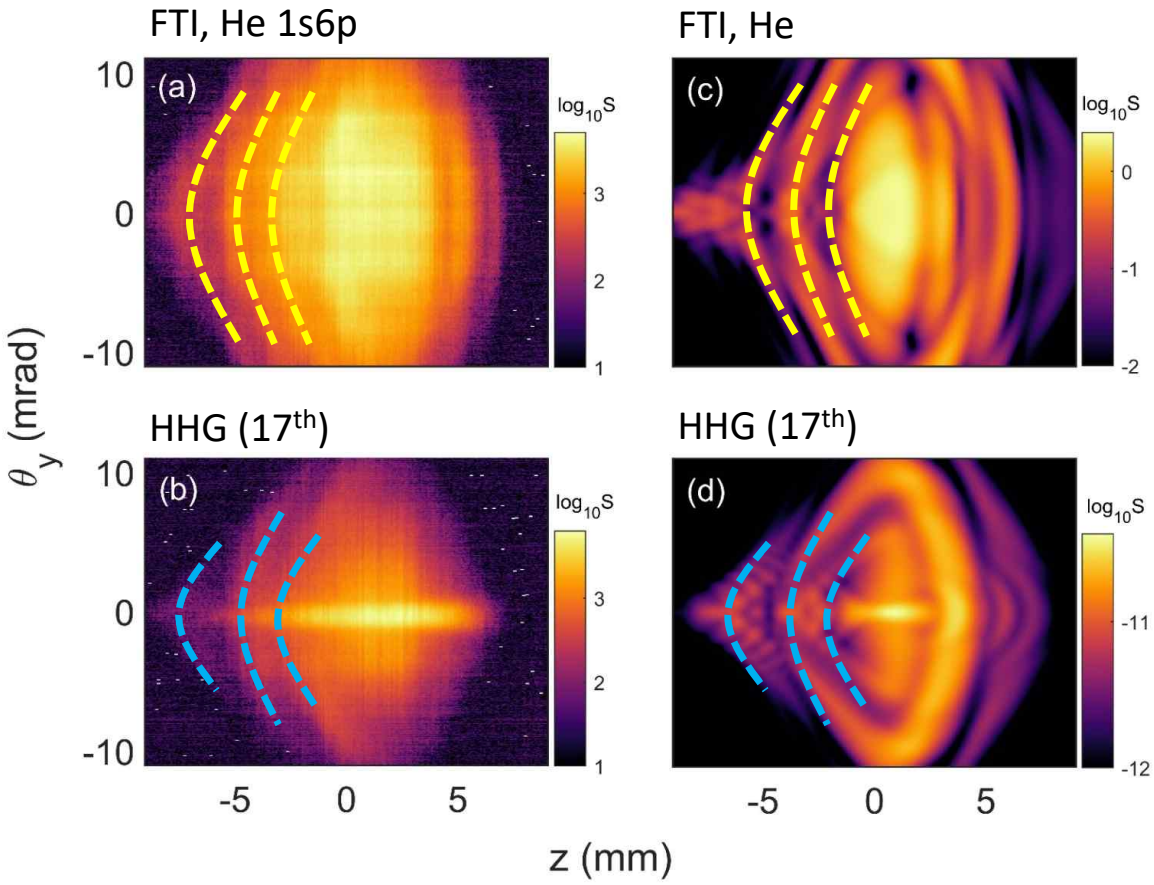

FTI spectrum looks similar to long trajectory harmonics!

CEP dependence

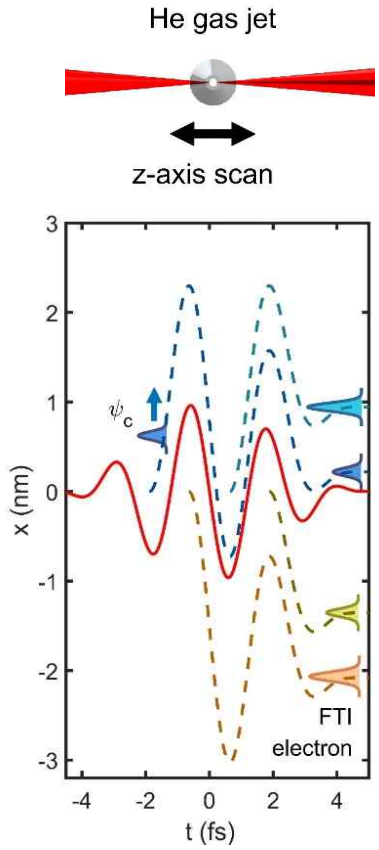

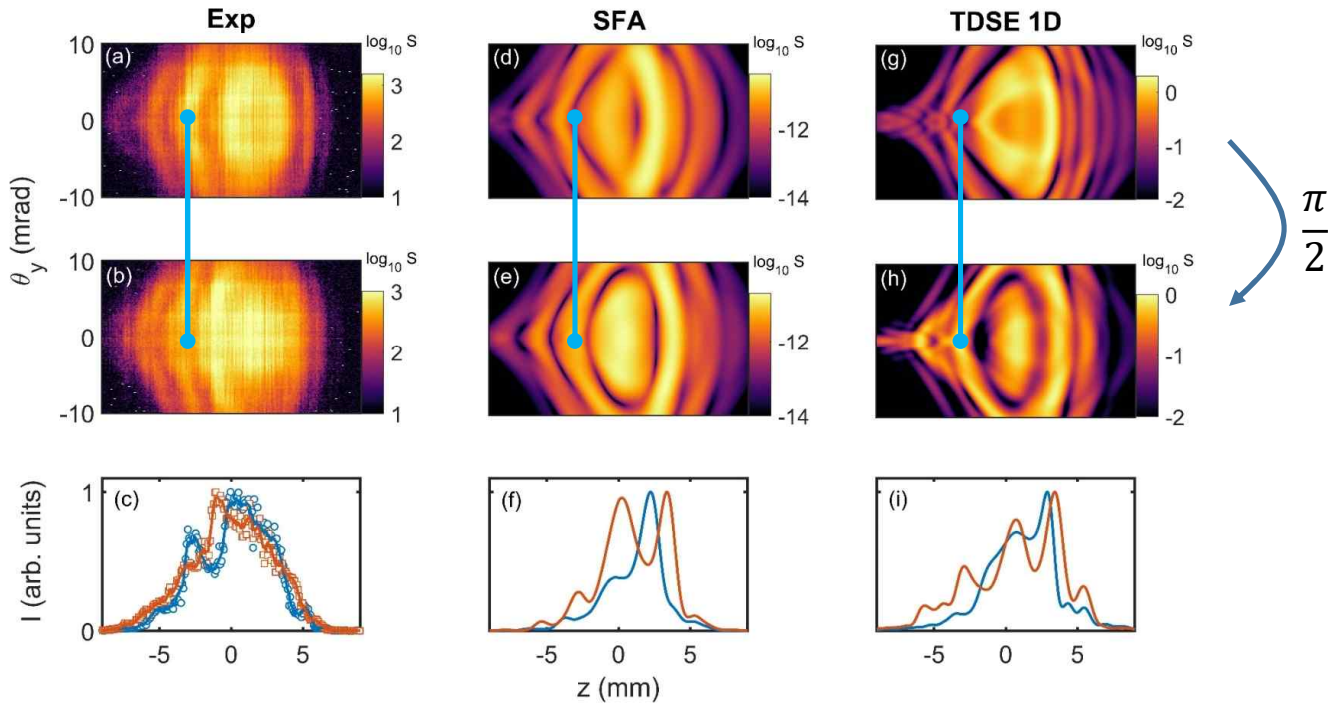

FTI emission can be coherently controlled just like HHG!

HHG -> interference of photons

FTI -> interference of electron wave packets

Summary

- Strong field physics
- ATI
- HHG
- FTI